

**NAA, EDXRF, CRYSTALLOGRAPHIC AND
VIBRATIONAL SPECTROSCOPIC STUDIES OF
MONOSODIUM GLUTAMATE**

PhD DISSERTATION

KHIN SWE OO

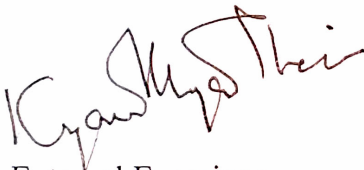
**DEPARTMENT OF PHYSICS
UNIVERSITY OF YANGON
MYANMAR**

JUNE 2004

**NAA, EDXRF, CRYSTALLOGRAPHIC AND
VIBRATIONAL SPECTROSCOPIC STUDIES OF
MONOSODIUM GLUTAMATE**

KHIN SWE OO

**THIS DISSERTATION IS SUBMITTED TO
THE BOARD OF EXAMINERS IN PHYSICS,
UNIVERSITY OF YANGON FOR THE DEGREE OF
DOCTOR OF PHILOSOPHY**



External Examiner

U Kyaw Mya Thein

MS Phys, MS Math (III)

Pro - Rector, UCS

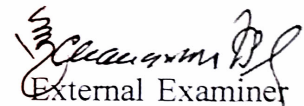


Chairman

Professor Dr Sein Htoon

CPhys FInstP (London)

**Head of Department of Physics
Yangon University**



External Examiner

Prof Dr SK Chakravarti

Dean & Head,

Applied Physics Dept,

NIT, Kurukshetra, India.

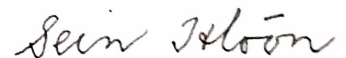


External Examiner

Dr. Ko Ko Oo PhD(Osaka)

Director

Department of Atomic Energy



Supervisor

Professor Dr Sein Htoon

CPhys FInstP (London)

**Head of Department of Physics
Yangon University**

CONTENTS

ABSTRACT

ACKNOWLEDGEMENTS

		Page
CHAPTER I	INTRODUCTION	1
1.1	Monosodium Glutamate (MSG)	1
1.2	Scientific Review	3
1.3	Anecdotal Evidence	4
1.4	Study of MSG	6
CHAPTER II	NEUTRON ACTIVATION ANALYSIS FOR MSG	8
2.1	Introduction to Neutron	8
2.1.1	Introduction	8
2.1.2	Neutron Production	9
2.1.3	Classification of Neutrons	10
2.2	Theory and Method	10
2.2.1	Fast Neutron Induced Reaction	10
2.2.2	Neutron Activation Analysis	11
	(i) Introduction	
	(ii) The NAA Method	
	(iii) Sensitivities Available	
	(iv) NAA with gamma Spectroscopy	
	(v) Special Features of FNAA Technique	
2.2.3	Methods of Neutron Measurement	17
	(i) Recoil Proton Method	
	(ii) Radio Activation Method	
2.3	Experimental	18
2.3.1	Experimental Facilities	18

2.3.1.1	Sources of Neutrons	18
	(i) Multivolt Pump Type Neutron Generator(NA150-04)	
	(ii) Isotropic Sources	
2.3.1.2	Gamma Rays Spectrometer System	20
	(i) Sodium Iodide NaI(Tl) Scintillation Detector	
	(ii) HPge Detector	
2.3.1.3	Parameter of Spectroscopy	23
	(i) Special Performance of Detector	
	(ii) Energy Calibration and Determination of Efficiency	
	(iii) Determination of Detector Efficiency	
	(iv) Neutron Flux Monitor	
2.3.2	Experimental Procedure	30
2.3.2.1	Sample Preparation	30
2.3.2.2	Sample Irradiation	30
2.3.2.3	Neutron Flux Determination	30
2.3.2.4	Determination for Cross-section of Na	31
2.3.2.5	Determination of Linear Absorption Coefficient of Na	32
2.3.2.6	Calculation of Experimental Sensitivity	32
2.4	Results and Discussion	36
2.4.1	Results	36
	(i) Cross Section Data for MSG(Monosodium Glutamate) Sample	
	(ii) Data for Sodium Content	
2.4.2	Discussion	37

CHAPTER III	ANALYSIS OF THE EDXRF METHOD	50
3.1	Introduction	50
3.2	The Shimadzu EDX 700 Spectrometer	54
3.3	Analysis of EDXRF Method	55
3.4	Experimental Set-up	56
3.5	Results and Discussion	57
3.6	Conclusion	58
CHAPTER IV	X RAYS DIFFRACTION AND CRYSTALLOGRAPHY	60
4.1	X ray Diffraction Technique (XRD)	60
4.2	Basic Principles of XRD	60
4.2.1	Types of XRD Techniques	63
4.3	X ray Powder Diffraction	67
4.4	Practical Aspects of the Method	69
4.5	Data Analysis and Interpretation	73
4.6	Crystal Lattice and Space Group Determination from X ray Powder Data	74
4.7	Sample Preparation	74
4.8	Comparison Against a Database of Known Materials	76
4.9	Quantitative Phase Analysis	76
4.10	Introduction to Crystallography	78
4.11	Crystal Systems	80
4.12	Diffraction of X rays by Crystal	81
4.12.1	Experimental Set Up	81
4.13	Results and Discussion	86

CHAPTER V	STRUCTURAL AND VIBRATIONAL ANALYSIS	89
5.1	Sample Preparation	89
5.2	FTIR Spectroscopy	89
5.3	Raman Spectroscopic System	93
5.4	Result and Discussion	95
5.5	Conclusion	98

REFERENCES

ABSTRACT

In this research, 14 Me V and 3 MeV neutron flux were determined by using foil activation method. NA 150-04 pump type Neutron Generator and Pu-Be source are used to irradiate the monosodium glutamate (MSG). High resolution HPGe dector and high efficiency NaI (TI) detector were used to detect gamma ray histogram in γ -ray spectroscopy. By using parameters of reaction, specific activity and elemental content of chemical compound were evaluated and compared with the actual content. The data agreed well with each other within experimental limits. The total cross - section of $^{23}\text{Na} (n,\alpha)^{20}\text{F}$ is very well agree with the evaluated nuclear data of JENDL - FF and SCINCROS II calculation and other data of SS - Nargolwalla with error bars. In EDXRF method, it was found that the major element is sodium only. But the elements of Sulphur (S), Strontium (Sr), Mercury (Hg), Lead (Pb), Arsenic (As) and Scandium (Sc), which are known as toxic elements, were not found in this sample. An attempt has been made to examine MSG crystallographically. Fourier Transform Infrared (FTIR-8400 Shimudsu) Spectrophotometer and R-2001 Raman System were used identify the significant vibration bands of molecular groups contained in MSG.

ACKNOWLEDGEMENTS

The author wish to express her gratitude and sincere thanks to her supervisor, Professor Dr Sein Htoon, PhD *Sur* CPhys FInstP *London*, Dean of Faculty of Engineering, Head of Department of Physics (IT), University of Yangon, for his invaluable help and advice (scientifically and socially), and effort during the course of this research.

The author wishes to thank Dr Tun Khin, MSc *Sur* PhD *Sur* DEM, Pro Rector, Yangon University and Head of Universities' Research Centre (URC) and Director of Asia Research Centre (ARC) for his help with EDXRF and FTIR measurements.

The author also wishes to express special thanks to Dr Pho Kaung, DSc(*Hokkaido*), Associate Professor, Department of Physics, University of Yangon for his valuable advice and supervision.

The author also wishes to express special thanks and deepest appreciation to Dr May Myint Si and Dr Kay Thi Thin, MSc PhD Ygn, Associate Professors, Department of Physics, University of Mandalay for their valuable advice and encouragement.

Thanks are also due to Dr Soe Myint, Lecturer, Department of Physics, Yangon University for his kind help with X-ray spectroscopy.

Last, but not least, I thank my parents, my father in law and my husband for their encouragement, help, assistance and patience during my research work.

CHAPTER I

INTRODUCTION

1.1 Monosodium Glutamate (MSG)

MSG, monosodium glutamate is a flavor enhancer. Accent is the primary U.S. brand name, and the Chinese version is called ve-tsin and other names are monosodium L-glutamate monohydrate, sodium glutamate monohydrate, Chinese seasoning, MSG, RL-50, Glutacyl and Glutavene.

Monosodium glutamate (MSG) is used as a flavor enhancer in a variety of foods prepared at home, in restaurants, and by food processors. Its use has become controversial in the past 30 years because of reports of adverse reactions in people who've eaten foods that contain MSG. MSG is the sodium salt of the amino acid glutamic acid and a form of glutamate. It is sold as a fine white crystal substance, similar in appearance to salt or sugar. It does not have a distinct taste of its own, and how it adds flavor to other foods is not fully understood. Many scientists believe that MSG stimulates glutamate receptors in the tongue to augment meat-like flavors.

Asians originally used a seaweed broth to obtain the flavor-enhancing effects of MSG, but today MSG is made by a fermenting process using starch, sugar beets, sugar cane, or molasses. Glutamate itself is in many living things: It is found naturally in our bodies and in protein-containing foods, such as cheese, milk, meat, peas, and mushrooms.

Some glutamate is in foods in a "free" form. It is only in this free form that glutamate can enhance a food's flavor. Part of the flavor-enhancing effect of tomatoes, certain cheeses, and fermented or hydrolyzed protein products (such as soy sauce) is due to the presence of free glutamate.

Hydrolyzed proteins, or protein hydrolysates, are acid-treated or enzymatically treated proteins from certain foods. They contain salts of free amino acids, such as glutamate, at levels of 5 to 20 percent. Hydrolyzed proteins are used in the same manner as MSG in

many foods, such as canned vegetables, soups, and processed meats. MSG has very little flavor of its own, but it 'improves' or enhances the flavor of other foods it is used with.

Research on the role of glutamate--a group of chemicals that includes MSG--in the nervous system also has raised questions about the chemical's safety.

Monosodium Glutamate is often used as a controversial food additive. Technically it is the sodium salt of glutamic acid, a naturally occurring amino acid which is produced in small quantities by the human body.

Some individuals seem to be sensitive to MSG, and exhibit what is known as 'Chinese Restaurant Syndrome' (because of its use in Asian cooking). The symptoms include headaches, chest pains, facial pressure, burning sensations, and sweating. The FDA (Food and Drug Administration) continues to list it as GRAS (Generally Recognized As Safe), but all foods containing MSG must state so on the label.

Studies have shown that the body uses glutamate, an amino acid, as a nerve impulse transmitter in the brain and that there are glutamate-responsive tissues in other parts of the body, as well. Abnormal function of glutamate receptors has been linked with certain neurological diseases, such as Alzheimer's disease and Huntington's chorea. Injections of glutamate in laboratory animals have resulted in damage to nerve cells in the brain. Consumption of glutamate in food, however, does not cause this effect. While people normally consume dietary glutamate in large amounts and the body can make and metabolize glutamate efficiently, the results of animal studies conducted in the 1980s. MSG and possibly some other glutamates can harm the nervous system?

A 1995 report from the Federation of American Societies for Experimental Biology (FASEB), an independent body of scientists, helps put these safety concerns into perspective and reaffirms the Food and Drug Administration's belief that MSG and related substances are safe food ingredients for most people when eaten at customary levels.

The FASEB report identifies two groups of people who may develop a condition the report refers to as "MSG symptom complex." One group is those who may be intolerant to MSG when eaten in a large quantity. The second is a group of people with severe,

poorly controlled asthma. These people, in addition to being prone to MSG symptom complex, may suffer temporary worsening of asthmatic symptoms after consuming MSG. The MSG dosage that produced reactions in these people ranged from 0.5 grams to 2.5 grams.

Although FDA has not fully analyzed the FASEB report, the agency believes that the report provides the basis to require glutamate labeling. FDA will propose that foods containing significant amounts of free glutamate (not bound in protein along with other amino acids) declare glutamate on the label. This would allow consumers to distinguish between foods with insignificant free glutamate levels and those that might contribute to a reaction.

1.2 Scientific Review

In 1959, FDA classified MSG as a "generally recognized as safe," or GRAS, substance, along with many other common food ingredients, such as salt, vinegar, and baking powder. This action stemmed from the 1958 Food Additives Amendment to the Federal Food, Drug, and Cosmetic Act, which required remarket approval for new food additives and led FDA to promulgate regulations listing substances, such as MSG, which have a history of safe use or are otherwise GRAS.

Since 1970, FDA has sponsored extensive reviews on the safety of MSG, other glutamates and hydrolyzed proteins, as part of an ongoing review of safety data on GRAS substances used in processed foods.

Scientific knowledge about how the body metabolizes glutamate developed rapidly during the 1980s. Studies showed that glutamate in the body plays an important role in normal functioning of the nervous system. Questions then arose on the role glutamate in food plays in these functions and whether or not glutamate in food contributes to certain neurological diseases.

One such review was by the FASEB Select Committee on GRAS Substances. In 1980, the committee concluded that MSG was safe at current levels of use but recommended

additional evaluation to determine MSG's safety at significantly higher levels of consumption.

In 1986, FDA's Advisory Committee on Hypersensitivity to Food Constituents concluded that MSG poses no threat to the general public but that reactions of brief duration might occur in some people. Also, the 1987 Joint Expert Committee on Food Additives of the United Nations Food and Agriculture Organization and the World Health Organization have placed MSG in the safest category of food ingredients.

A 1991 report by the European Communities' (EC) Scientific Committee for Foods reaffirmed MSG's safety and classified its "acceptable daily intake" as "not specified," the most favorable designation for a food ingredient. In addition, the EC Committee said, "Infants, including prematures, have been shown to metabolize glutamate as efficiently as adults and therefore do not display any special susceptibility to elevated oral intakes of glutamate."

A 1992 report from the Council on Scientific Affairs of the American Medical Association stated that glutamate in any form has not been shown to be a "significant health hazard."

1.3 Anecdotal Evidence

Many of these safety assessments were prompted by unconfirmed reports of MSG-related adverse reactions. Between 1980 and 1994, the Adverse Reaction Monitoring System in FDA's Center for Food Safety and Applied Nutrition received 622 reports of complaints about MSG. Headache was the most frequently reported symptom. No severe reactions were documented, but some reports indicated that people with asthma got worse after they consumed MSG. In some of those cases, the asthma didn't get worse until many hours later.

Also, several books and a TV news show have reported widespread and sometimes life-threatening adverse reactions to MSG, claiming that even small amounts of manufactured glutamates may cause adverse reactions.

Prompted by continuing public interest and a flurry of glutamate-related studies in the late 1980s, FDA contracted with FASEB in 1992 to review the available scientific data. An unknown percentage of the population may react to MSG and develop MSG symptom complex, a condition characterized by one or more of the following symptoms:

- burning sensation in the back of the neck, forearms and chest
- numbness in the back of the neck, radiating to the arms and back
- tingling, warmth and weakness in the face, temples, upper back, neck and arms
- facial pressure or tightness
- chest pain
- headache
- nausea
- rapid heartbeat
- bronchospasm (difficulty breathing) in MSG-intolerant people with asthma
- drowsiness
- weakness.

In otherwise healthy MSG-intolerant people, the MSG symptom complex tends to occur within one hour after eating 3 grams or more of MSG on an empty stomach or without other food. A typical serving of glutamate-treated food contains less than 0.5 grams of MSG. A reaction is most likely if the MSG is eaten in a large quantity or in a liquid, such as a clear soup.

- Severe, poorly controlled asthma may be a predisposing medical condition for MSG symptom complex.
- No evidence exists to suggest that dietary MSG or glutamate contributes to Alzheimer's disease, Huntington's chorea, amyotrophic lateral sclerosis, AIDS dementia complex, or any other long-term or chronic diseases.
- No evidence exists to suggest that dietary MSG causes brain lesions or damages nerve cells in humans.

- The level of vitamin B6 in a person's body plays a role in glutamate metabolism, and the possible impact of marginal B6 intake should be considered in future research.
- There is no scientific evidence that the levels of glutamate in hydrolyzed proteins causes adverse effects or that other manufactured glutamate has effects different from glutamate normally found in foods.

Following is another list of well-documented reactions to monosodium glutamate. Individuals with extreme sensitivities may experience seemingly incurable fibromyalgia-type pain, while others may have immediate, acute reactions, including heart attack. A high enough dose is toxic to anyone which is far more likely as more and more foods contain higher percentages of MSG: headaches, migraines, stomach upset, nausea and vomiting, diarrhea, irritable bowel syndrome, asthma attacks, shortness of breath, anxiety or panic attacks, heart palpitations, partial paralysis, heart attack-like symptoms, balance difficulties, mental confusion, mood swings, neurological disorders (Parkinson's, MS, ALS, Alzheimer's), behavioral disorders (especially in children and teens), allergy-type symptoms, skin rashes, runny nose, bags under the eyes, flushing, mouth lesions, depression and more .

Under current FDA regulations, when MSG is added to a food, it must be identified as "monosodium glutamate" in the label's ingredient list. Each ingredient used to make a food must be declared by its name in this list. While technically MSG is only one of several forms of free glutamate used in foods, consumers frequently use the term MSG to mean all free glutamate.

1.4 Study of MSG

In this research the contamination of Na in MSG is determined by NAA (Neutron Activation Analysis) method, EDXRF (Energy Dispersive X ray Fluorescence) method and other factors of the MSG crystal investigated in crystallographic point of view. The Powder method is also used for identifying substance. Fourier Transform Infrared (FTIR-

8400 Shimadzu) Spectrophotometer and R-2001 Raman System were used to identify the significant vibration bands of molecular groups contained in MSG.

Nuclear Physics techniques often have a great advantage over traditional chemical techniques for the determination of elemental composition of materials. Two techniques in particular have become widely used: EDXRF (Energy Dispersive X ray Fluorescence) and NAA (Neutron Activation Analysis).

X ray powder diffraction is used to determine the atomic structure of crystalline materials. X ray powder diffraction is an old technique, in use for most of this century. The capabilities of the technique have recently grown for two main reasons: (i) development of X ray sources and optics and (ii) the increasing power of computers and software for analysis of powder data. A few structures of organic compounds have been determined with full accuracy.

EDXRF is also used for analysis of small quantities of element. In this technique, a thin sample of the material is placed in the secondary target area of X ray tube and bombarded with secondary X rays.

Moreover, neutron flux and cross-section is determined by NAA method. In NAA technique, a small sample of the material to be evaluated is exposed to a flux of neutrons (14MeV) from the Neutron Generator and the flux of neutrons (3MeV) from Pu-Be source. Nuclei of stable elements can become radioactive through the neutron capture (n,γ) reaction. Many of these radioactive nuclei decay through β and subsequent γ emission, and the γ rays are characteristic of that particular decay process. Activation analysis achieves a qualitative and quantitative analysis of an unknown sample by irradiating the sample thus producing radioactive nuclides from stable or unstable isotopes present in the sample.

To study the nuclear reactions in detail, it is necessary to have a quantitative measurement of the probability of a given reaction is called cross-section. Neutron activation cross-section data are also important in the fusion reaction technology. In general, knowledge of fast neutron induced reaction is of importance in basic nuclear

theory, in applications of fast neutron activation analysis, and fusion and fission reactor technology. Cross-sections of neutron induced reaction depends on the energy of the incident neutrons. In the case of accurate measurement, the neutron flux of the neutrons with the energy of 14MeV and 3MeV is the one of the important factor for a certain reaction.

When determination of the elemental content of some chemical compound one used the sample comparative method. In here, known concentration chemical compound NaCl and Na₂CO₃ were applied as standard samples.

CHAPTER II

NEUTRON ACTIVATION ANALYSIS FOR MSD

2.1 Introduction to Neutron

2.1.1 Introduction

For many experimental investigations in neutron physics and applications of fast neutron activation analysis, it is essential to know the yield of the neutron sources as well as flux distribution patterns around it.

The knowledge of the flux density distribution is needed to optimize the position of samples to be irradiated for activation cross section measurements, activation analysis and radiation effect studies. In the case of point-like source the flux density can change significantly inside an extended sample. Therefore to estimate the average dose the spatial distribution of the flux should be determined by experiment in the vicinity of the sources. The distributing effect of the scattered neutrons can be eliminated by using activation detectors with high reaction thresholds.

As a part of this research with the neutron sources, the neutron flux was determined by using natural copper foils undergo the (n, 2n) reactions. Empirical sensitivity data have been obtained for some elements, under standard irradiation and counting condition by irradiation a known weight of either the element or a pure compound of the element. The weight of sample used for these tests was dependent on the neutron cross section of sample element. During the test decade, the neutron generator has contributed significantly to analytical programs in much research academic and industrial laboratories. In its capacity as a tool for activation analysis, the principal emphasis has been on the use of 14 MeV neutrons. The preferential use of 14 MeV neutrons is dictated primarily by the high neutron flux obtained from ${}^2\text{H}({}^3\text{H}, n){}^4\text{He}$ reaction.

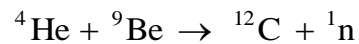
To explore the utility of 3 MeV, neutron activation analysis, γ rays spectra of most of the elements, irradiated with 3 MeV neutrons were systematically investigated. The results of this study have been applied to compositional analysis in 14 MeV neutrons activation

analysis. This buildup is due to neutron production from interaction of the primary deuteron beam with deuterons embedded in a tritium target from previous irradiation.

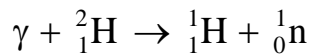
In addition to the experimental sensitivities detailed information and counting geometries, sample attenuation corrections and detector efficiencies have been induced to facilitate expected sensitivity calculations for other systems on a semi-quantitative basis.

2.1.2 Neutron Production

The existence of the neutron was predicted, as early as 1911 but in late 1932 Chadwick showed that by using reaction, the neutrons exist inside the nucleus.

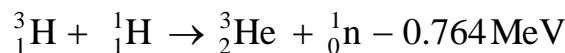
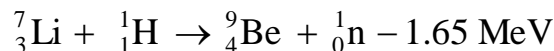
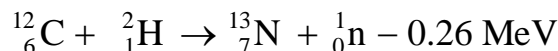
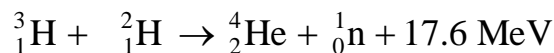
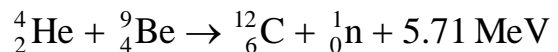


The particle so produced cannot be deflected by electric and magnetic fields and one concluded that the particle must be charge less particle. In 1934, the now accepted value for m_n , which is 1.008983 u, was obtained by Chadwick and Goldhaber by using a still more precise method.



Nuclear reactions are the only source of neutron and on light elements $A < 25$ the (γ, n) reaction are still used to produce these particles.

Neutrons are produced by the following reactions.



In order to obtain monoenergetic neutrons photo neutron sources are used. Most of the sources are based on the reactions ${}^9\text{Be}(\gamma, n){}^8\text{Be}$ and ${}^2\text{H}(\gamma, n){}^1\text{H}$.

Neutrons can also be produced in particle accelerator such as Vande Graaff electrostatic generator. The reaction ${}^2\text{H}(d, n){}^3\text{He}$ is exoergic, with a Q-value of 3.28 MeV. A good neutron yields which are the numbers per second from 1 g of target at 1 cm one curie of the source can be obtained if the conditions of the experiments are carefully controlled.

Another reaction that can be used is ${}^3\text{H}(d,n){}^4\text{He}$ with a Q-value of 17.6 MeV. The neutrons produced by the methods discussed above have intermediate or high energies in the range 5 keV to 20 MeV.

2.1.3 Classification of Neutrons

The importance of neutron energy in the interaction of neutrons with matter makes necessary a classification of neutrons. Neutrons are roughly classified into four distinct groups according to their energies. There are:

- (i) Thermal neutrons
- (ii) Intermediate neutrons
- (iii) Fast neutrons
- (iv) High energy neutrons

Generally, thermal neutrons have energies less than 1eV, and they are in thermal equilibrium with their surroundings. The elastic scattering and fission processes are significant in the interaction of thermal neutrons with matter. The intermediate neutron energy region is between thermal energy and nearly 10 keV. Since the neutron absorption exhibits sharp resonances in this region, these neutrons are usually termed as resonance neutrons. The capture reaction process occurs with a very high probability for a number of nuclides at particular energies in this region.

The fast neutron region is from resonance up to about 1 – 20 MeV. The nuclear reactions in this region usually vary rather slowly with energy, but a greater variety of reactions become possible.

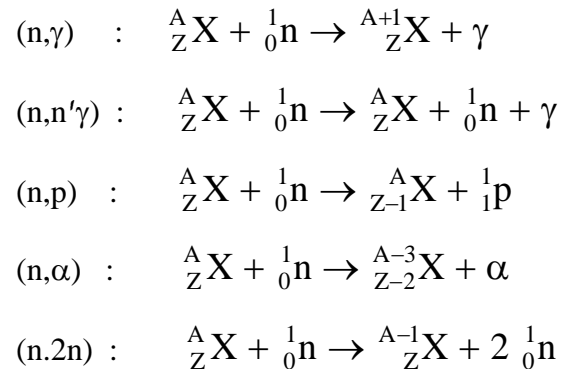
The region of neutron energies above 20 MeV has no well-established title. However, the neutrons in this region are distinguished from other fast neutrons by the fact that particles of this energy show relativistic effects. For this reason, these neutrons with energies around 100 MeV or higher may cause the emission of a shower of many different types of particles.

2.2 Theory and Method

2.2.1 Fast Neutron Induced Reaction

Neutrons, because they are uncharged heavy particles, have properties that make them especially interesting and important in contemporary science and technology. Neutrons have direct uses as research tools, for example, their optical properties make them more useful than X-rays for certain analytical purposes.

Neutrons do not directly ionize the matter through which they pass. Therefore, neutrons are measured indirect way using some reactions. Some nuclear reactions produced by fast neutrons are described below. The principal nuclear reactions in activation analysis with fast neutrons are:



In the present work, (n,2n) reaction is used for flux calculation of natural copper foils. The mass change in this reaction is always s negative and fast neutrons are needed to bring about these endoergic reactions. In ${}^{63}\text{Cu}(n,2n){}^{62}\text{Cu}$ reaction, the threshold energy ($E_\gamma = 0.511$ MeV) is 12 MeV, so that low energy neutrons are cut off. ${}^{62}\text{Cu}$ has a half-life of 9.8 minutes.

2.2.2 Neutron Activation Analysis

(i) Introduction

Neutron activation analysis (NAA) is a sensitive analytical technique useful for performing both qualitative and quantitative multi-element analysis of major, minor, and trace elements in samples from almost every conceivable field of scientific or technical interest. For many elements and applications, NAA offers sensitivities that are superior to

those attainable by other methods, on the order of parts per billion or better. In addition, because of its accuracy and reliability, NAA is generally recognized as the "referee method" of choice when new procedures are being developed or when other methods yield results that do not agree.

The basic essentials required to carry out an analysis of samples by NAA are a source of neutrons, instrumentation suitable for detecting gamma rays, and a detailed knowledge of the reactions that occur when neutrons interact with target nuclei. Brief descriptions of the NAA method, reactor neutron sources, and gamma-ray detection are given below.

When an atom emits a photon, the energy of the photon equals the difference between the energies of the initial and final states. By measuring photon energies it is possible to infer the chemical nature of the emitting atoms. Spectroscopic analysis exploits this principle.

An analogous situation exists with nuclei. Like an atom, the quantized energy states of a nucleus are unique. When a nucleus emits a photon the energy of the photon equals the difference between the energies of the initial and final nuclear states. By measuring the photon energies it is possible to identify the emitting nuclei. The primary difference between the atomic and nuclear analyses is one of energy scale; photons emitted by atoms have energies in the electron volt range. Photons emitted by nuclei have energies in the MeV range. This places the nuclear photons in the gamma region of the electromagnetic spectrum.

Neutron activation analysis takes advantage of the unique relation between photon energy and the emitting nucleus. *Neutron activation* means that nuclei have been made radioactive by bombardment with neutrons. *Analysis* refers to the measurement of the energies of the gamma photons released in the radioactive decay processes.

There are three steps involved in neutron activation analysis:

1. A nucleus captures a neutron, forming an unstable isotope.
2. The unstable isotope undergoes beta decay, producing a product nucleus in an excited state.
3. The excited state decays by gamma photon emission.

The experiment involves the following steps:

- (1) We first identify the emitting nucleus by measuring the gamma photon energies.
- (2) Knowing that the nucleus was formed by beta decay, we then identify the isotope that led to the beta decay.
- (3) Knowing that this isotope was formed by neutron capture, we finally work backward to identify the nucleus that initiated the sequence.

Neutron activation analysis makes it possible to determine the *concentration* of the initial isotope. To do this, we prepare two identical samples. One is known percentage of the element of interest and another one is which we want to know the percentage of the same element. Both samples are irradiated simultaneously with a rain of neutrons from the neutron sources. We then measure the gamma photon activities of the two samples. The ratio of the activities of the gamma photons is equal to the ratio of the concentration of the isotopes.

By exposing two samples to the same neutron source and by taking the ratio of the induced activities, we need not know

- (1) how many neutrons actually impinged on the samples, nor
- (2) the probability that the neutrons are captured by the nuclei of interest.

These are very important features of neutron activation analysis.

It is the great sensitivity of neutron activation analysis that makes the technique so useful. In many instances it is possible, using only a tiny sample, to determine concentrations equivalent to 1 atom of interest in the presence of 1 billion other atoms. Environmentalists, criminologists, and analytical chemists, all of whom must often analyze samples for trace amounts (very small quantities) of impurities, use neutron activation analysis to great advantage.

(ii)The NAA Method

The most common type of nuclear reaction used for NAA is the neutron capture or (n, γ) reaction. When a neutron interacts with the target nucleus via a non-elastic collision, a compound nucleus forms in an excited state. The excitation energy of the compound nucleus is due to the binding energy of the neutron with the nucleus. The compound nucleus will almost instantaneously de-excite into a more stable configuration through emission of one or more characteristic prompt gamma rays. In many cases, this new configuration yields a radioactive nucleus which also de-excites (or decays) by emission of one or more characteristic delayed gamma rays, but at a much slower rate according to the unique half-life of the radioactive nucleus. Depending upon the particular radioactive species, half-lives can range from fractions of a second to several years.

In principle, therefore, with respect to the time of measurement, NAA falls into two categories: (1) prompt gamma-ray neutron activation analysis (PGNAA), where measurements take place during irradiation, or (2) delayed gamma-ray neutron activation analysis (DGNAA), where the measurements follow radioactive decay. The latter operational mode is more common; thus, when one mentions NAA it is generally assumed that measurement of the delayed gamma rays is intended. About 70% of the elements have properties suitable for measurement by NAA.

(iii)Sensitivities Available

The sensitivities for NAA are dependent upon the irradiation parameters (i.e., neutron flux, irradiation and decay times), measurement conditions (i.e., measurement time, detector efficiency), nuclear parameters of the elements being measured (i.e., isotope abundance, neutron cross-section, half-life, and gamma-ray abundance). The accuracy of an individual NAA determination usually ranges between 1 to 10 percent of the reported value. Table 2.1 lists the approximate sensitivities for determination of elements assuming interference free spectra.

Estimated detection limits for INAA using decay gamma rays. Assuming irradiation in a reactor neutron flux of $1E11$ neutrons per square centimeter per second.

(iv) NAA with γ - ray Spectroscopy

Neutron activation analysis was first applied by Harvesy and Levi in 1937. Neutron Activation Analysis (NAA) is a non- destructive trace element technique capable of measuring up to 64 elements, many at levels of 1 $\mu\text{g}/\text{kg}$ or lower. The sample is placed in a flux of neutrons and after removal the emissions of the radionuclide produced are measured.

The sample is placed in one of the irradiation sites which bathe the sample in a flux of neutrons and the elements within the sample absorb an extra neutron to produce γ - ray emitting radionuclides. The sample is removed from the reactor either manually or using one of the automated pneumatic systems and The general character of the variation of the radiation intensity with thickness of the absorber is γ -rays spectrometry is then used to identify the elements present and with the use of certified standards, to accurately determine the concentration.

Table 2.1 Approximate sensitivities for determination of elements

Sensitivity (nanograms)	Elements
0.1	Dy, Eu
0.1 - 1	In, Lu, Mn
1 - 10	Au, Ho, Ir, Re, Sm, W
10 - 100	Ag, Ar, As, Br, Cl, Co, Cs, Cu, Er, Ga, Hf, I, La, Sb, Sc, Se, Ta, Tb, Th, Tm, U, V, Yb
100 - 1E3	Al, Ba, Cd, Ce, Cr, Hg, Kr, Gd, Ge, Mo, Na, Nd, Ni, Os, Pd, Rb, Rh, Ru, Sr, Te, Zn, Zr
1E3 - 1E4	Bi, Ca, K, Mg, P, Pt, Si, Sn, Ti, Tl, Xe, Y
1E4 - 1E5	F, Fe, Nb, Ne
1E6	Pb, S

For solid sample, NAA can be used to analyze a wide variety of materials and is particularly suited to the analysis of solids since they can be analyzed as is, without the necessity of dissolution of the sample. Plastics, carbon fiber, graphite and boron compounds which are highly insoluble are easily analyzed by NAA. For liquid samples of up to 30 ml in volume can be analyzed provided the boiling point is greater than 60 C.

For organic materials, which consists of any the following elements: carbon, hydrogen, oxygen and nitrogen present an ideal sample matrix for NAA since they do not produce significant γ -ray emitting radionuclides. Therefore, upon irradiation the only γ -ray emissions measured are from impurities and/or additives in the sample. For Halide; NAA is especially sensitive in the determination of the halide: chlorine, bromine and iodine which can be measured down to 10 $\mu\text{g}/\text{kg}$; fluorine is not so sensitive but can be measured at concentrations down to 1mg/kg. For volatile elements, since NAA does not require any sample pre-treatment it is very useful in the determination of volatile elements such as arsenic, selenium, cadmium and mercury which may be lost during the pre- treatment required by other analytical techniques. NAA is a non-destructive technique and therefore after the activated radionuclide has been allowed to decay the sample can be re-analyzed or archived. For this reason NAA has been used in forensic analysis.

(v) Special Features of FNAA Technique

The advantages of fast neutron activation analysis have been described many times and will only be outlined here. First, the technique is very sensitive and accurate. Secondly, it does not result in contamination by reagents. Thirdly, the activated isotope can be positively identified by more than one characteristic property such as, half- life, gamma spectrum or maximum beta energy. So that, there is a build-in check on accuracy. Fourthly it is at least mechanically non-destructive, so that a sample can be analyzed repeatedly without removing it from its container. Fifthly, it requires only minimal sample preparation.

The advantages of FNAA include the following items. Because it has lower flux density compared to that of thermal neutron activation analysis it does not give desired sensitivity for certain elements. It has no great advantages and other techniques are more suitable for few elements with low cross-section for fast neutrons.

2.2.3 Methods of Neutron Measurement

Two general methods used in modern laboratories are:

- (i) Recoil proton method and
- (ii) Radio activation method

(i) Recoil proton method

The foundation of this method rests on the knowledge of the cross sections of neutron – proton scattering. In this method, reaction events are counted through the determination of number of product particles (proton) giving off in the reaction. This has to be done on-line and usually not only the number of product but also their energy spectrum and the angular distribution have to be measured. The various types of detectors can be used but organic scintillation detector. It is more complicated than the radio activation method due to the behavior of scattered neutron cross-section, isotropic angular distribution, recoil proton energy, incident neutron direction, etc.

(ii) Radio Activation Method

The radio activation method is best studied to measure the neutron flux. The key to radio activation method of determining neutron flux is to select a detector whose half-life gives sufficient proof that the particular reaction sought occurs.

In order to measure neutron fluxes by activation techniques, there are several useful neutron reactions which results in a radioactive product. There are the (n,γ) , (n,p) , $(n,2n)$, (n,d) and (n,f) reactions.

The choice of detector will be determined which technique to use for a flux determination. Activation technique is based on the irradiation of a chosen sample foils by neutron and lead to radioactive residual nucleus. The activities produced by this residual nucleus are measured by absolute β - counting or γ - counting. The use of spectroscopic ally pure foils leads to higher precision nowadays.

In this case, the following parameters are important:

- (i) half-life of the isotope
- (ii) abundance and reaction cross-section for the fast fraction of the isotope.

In this research, the natural copper foils of spectroscopic ally pure are used for $^{63}\text{Cu}(n,2n)^{62}\text{Cu}$ reactions. These reactions are chosen because of their suitable parameters for measuring instrument in our laboratory. Activation method is a recent addition for such investigation in modern laboratories for its properties of fast, accurate and easy to measure.

2.3 Experimental

2.3.1 Experimental Facilities

2.3.1.1 Sources of Neutrons

Unlike the case for gamma rays and alpha and beta particles, there are no practical radioisotope sources for neutrons; they are not produced by any of the traditional radioactive decay processes. However, there are several methods by which neutrons may be produced:

The neutron sources, widely used in nuclear physics investigations, can be categorized by:

1. Isotropic source
2. Spontaneous fission neutron sources
3. Photo neutron sources
4. Neutron generator and
5. Research reactor

Plutonium and uranium isotopes decay by alpha particle emission. The alpha particle is absorbed by the nuclei of the low atomic number elements (N, O, F, C, Si, etc.) and a neutron is produced. The yield depends upon the chemical composition of the matrix and the alpha production rate for plutonium and uranium. Neutrons from (α,n) reactions are produced randomly (not time-correlated) and they exhibit a broad energy spectrum.

The even-numbered isotopes of plutonium (^{238}Pu , ^{240}Pu , and ^{242}Pu) spontaneously fission (SF) at a rate of 1100, 471, and 800 SF/gram-second respectively. Like (α,n) neutrons, SF neutrons have a broad energy spectrum. SF neutrons are time-correlated (several neutrons are produced at the same time), with the average number of neutrons per fission being

between 2.16 and 2.26. Uranium isotopes and odd-numbered plutonium isotopes spontaneously fission at a much lower rate (0.0003 to 0.006 SF/gram-second).

In this research work, the two neutron source facility can be obtained:

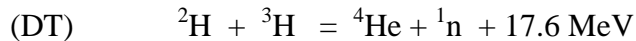
(i) Multivolt Pump type Neutron Generator (NA 150-04) and (ii) Isotropic sources

(i) Multivolt Pump Type Neutron Generator (NA 150-04)

A pump type neutron generator (NA 150-04) which is supported by IAEA capable of accelerating atomic deuterium ions up to 150 keV was used. In general, the neutrons are excited under radio frequency in the ion source and extracted into high vacuum multi-electrode high voltage particle accelerator. The fast neutrons are produced by accelerated deuterons strike the tritium target composed a copper disc after passing through the beam focusing electrodes.

During the running time the target and turbo molecular pump for high vacuum are always running at the same cooling water temperature.

The maximum beam current obtainable is 2mA and the neutron output yields $\sim 5 \times 10^{10}$ neutrons per second with 1mA beam current. The Vande Graaff accelerator is used exclusively for production of 14MeV neutron from the nuclear reacting.



(ii) Isotropic sources

Isotropic neutron sources have been utilized for experimental neutron research work in the Nuclear research Laboratory of the Department of Physics, University of Yangon, since 1968.

As a neutron source, a Pu-Be source was used. ${}^{239}\text{Pu}$ decays with a half-life of 42300 years and emit α 's of energies 5.15, 5.13 and 5.10 MeV. Pu can be alloyed with Be as Pu-Be to make a convenient neutron source. The Pu-Be source has several advantages, namely:

- (1) the alloying of Pu with Be makes the source homogeneous and reproducible,
- (2) no penetrating g-rays is emitted and

(3) the very long half life.

The disadvantages lies in the small yield and in the fact that a Pu-Be source may emit extra neutrons from the fission of Pu if the source is brought into a neutron field.

Another isotope neutron source used in Pu-Be which carrying 3 MeV neutrons are produced by the following reaction.



It obtained from USSR through IAEA was used in this present work. It has dimensions of 2.1 cm in diameter by 3.3 cm in length. The neutron output from the capsulated Pu-Be source is $(1.66 \pm 0.12) \times 10^6$ neutron/ sec.

2.3.1.2 Gamma Ray Spectrometer system

A typical spectrometer system comprises a detector which creates analog pulses, the usually HV power supply, preamplifier and amplifier (which must be linear to preserve the proportionality between pulse height and energy) and a pulse height analyzer. The pulse height analyzer can be a single channel analyzer (SCA) or a multichannel analyzer (MCA).

Photon spectrometry, and especially gamma rays spectrometry, is the most widely used pulse height spectrometric technique. Detectors transform the radiation energy into electronic pulses, the preamplifier followed up these pulses by making impedance matching and put into the main amplifier.

The duty of main amplifier is amplifying, shaping and rejecting the pulses and feeding to the analog to digital converter portion of multichannel analyzer. Multichannel analyzer effectively measures the counts in many energy channels simultaneously. Then the spectrum histogram of intensities and pulse height (voltage) is recorded by the Maestro 32 version 5.1. The block diagram of gamma- ray spectrometer is shown in Fig 2.1.

(i) Sodium Iodide NaI(Tl) Scintillation Detector

One of the most efficient methods of counting γ -rays and measuring their energies is the detection by a scintillation gamma-rays spectrometer. The scintillation detector consist of a scintillator coupled optically to a photomultiplier tube which is connected through a suitable preamplifier and an amplifier to either pulse height analyzer or to scalar. The scintillator used in the present work is a thallium activated sodium iodide crystal, NaI(Tl). The size of the crystal is 3" x 3".

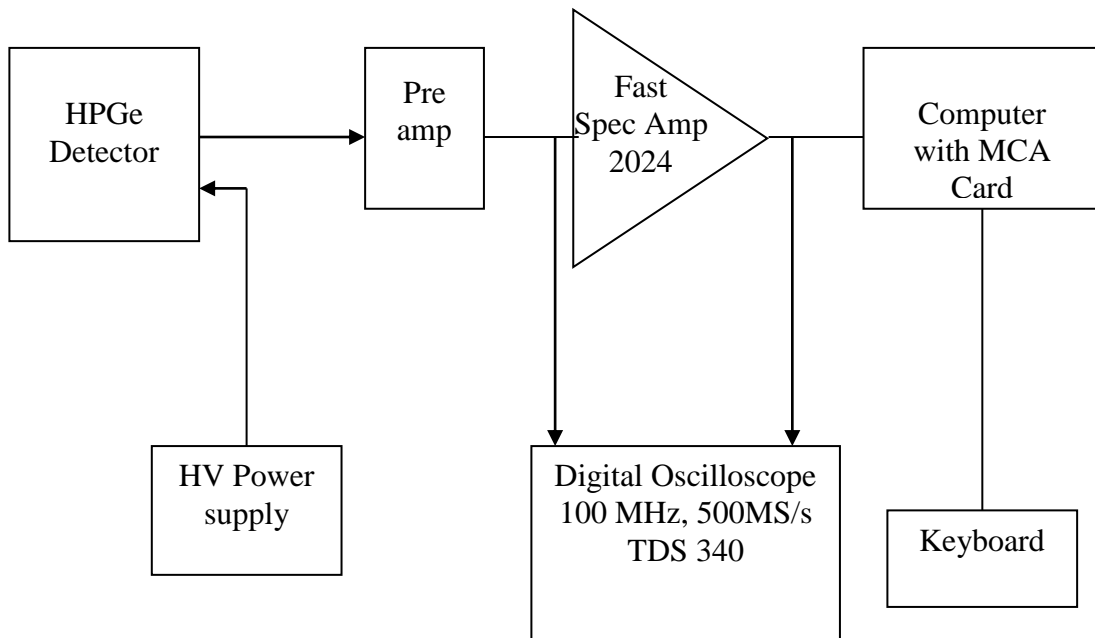


Fig.2.1 The block diagram of gamma ray spectroscopy

In operation of the scintillation detector system, nuclear radiation incident on the scintillator losses its energy by causing ionization and excitation within the crystal. A fraction of this energy is converted into light photons radiating in all directions. The resolution is 9.8% by using the 1.173 MeV peak of ^{60}Co (standard source) which has half-life of 5.268 years.

(ii) HPGe Detector

The most common material used for semiconductor radiation detector is germanium. It is grown in pure state (10^{14} impurities per cm^3 Ge(Li) materials) and in high purity quantity (10^{10} imp/cm³ IG material). Lithium ions can be drifted into both Si and Ge crystal to produce useful detectors because the level of uncompensated impurities in the applications Si(Li) detectors are limited to the opposite extreme of low energy gamma rays or X rays.

Without lithium compensation step, high resistivity and detection depth 10 cm can be reached by using reverse bias 1000V. This large volume Ge diode detectors are usually called "intrinsic Ge" or "high purity Ge" (abbreviated HPGe) detectors.

The bulk of the high purity material is generally p-types: this configuration is referred to as n⁺-p-p⁺ diode structure. The detector depletion region is formed by reverse biasing this n⁺-p junction. The depletion region effectively begins at the n⁺ edge of the central region, and extends further into the p⁺ region as the active volume extends all the way from one contact to the other and the electric field sufficient high to impart saturation velocity to the charge carriers, minimizing the collection time and the detrimental effects due to recombination and trapping.

To reduce noise, avoid potential contamination of the detector surface from any residual vapors within the detector vacuum housing and maintain lithium stability, Ge(Li) and HPGe detectors are enclosed and operated in the vacuum cryostat which provides thermal contact between the Ge crystal and a reservoir of liquid Nitrogen(LN₂) at a temperature of 77K.

In this research, HPGe detector was used for its high energy resolution better than other detectors such as NaI(Tl) scintillation detector and silicon detector and it can be stored at room temperature when no operation.

2.3.1.3 Parameter of Spectroscopy

(i) Special Performance of Detector

The important properties of the detector will be determined:

- Energy Resolution
- Detector Efficiency

- Peak Shape and Peak to Compton Ratio

as a function of gamma ray energy and counting rate.

Energy Resolution

Energy resolution is one of important parameters frequently used to judge the quality of detector and a measure of the width of the peak. It is defined as the full-width of the peak at one half of the maximum height (Full Width at Half Maximum height FWHM). The FWHM is given either in energy or when divided by the energy of the peak and multiplied by 100 is expressed as percent resolution.

The factors determining the resolution of a detector include:

- the type of detector
- the size of detector
- quality of the detector

The resolution of a particular detector is also usually dependent on the bias voltage. Therefore, it is important to understand how variations in the bias voltage affect the resolution and operation of the detector and how to determine the optimum operating voltage for any system.

Detector efficiency

Three types of detector efficiencies are commonly used: absolute, intrinsic, and absolute peak efficiency.

Absolute efficiency is defined as the number of events recorded divided by the number of radiations emitted by the source. Not also that this definition depends on the solid angle that the detector presents to the source and is strongly dependent on the source detector distance, especially when the source is close to the detector.

Intrinsic efficiency is defined as the number of events recorded divided by the number of radiations incident on the detector. One might think that the intrinsic efficiency should be independent of the source detector geometry but if one defines the detector as the outside of the cover instead of the active region, and then there may still be some dependence on the source detector separation.

Peak efficiency is defined as the number of events recorded in the peak compared to the total number of events recorded.

The efficiency of the detector depends not only on the size of the detector but also on the energy of the radiation.

Peak Shape and Peak to Compton Ratio

By using the amplifier in the experiment, one can shape the signal in a classical Gaussian shape. If the peak has a true Gaussian shape, the ratio of the FWTM to FWHM will be equal to 1.823. A detector with good peak-to-Compton ratio is a first demand when measuring this type of sample. The Compton continuum for 1.33 MeV gamma ranges from 0 to 1.118 MeV. The value is obtained by dividing the height of the 1.33 MeV photopeak by the average Compton Plateau between 1.040 and 1.096 MeV.

(ii) Energy Calibration and Determination of Efficiency

The electronics set-up for counting system is shown in Fig. 2.4. The detector bias was supplied by EHT unit (model 3002, ORTEC) at 3 kV. The preamplifier output pulses were fed into the multichannel analyzer (Maestro 32 version 5.1) which has a conversion gain of 4096 channels. Amplifier was set for output pulse of unipolar shape with a time constant of 1 μ s. By using the Maestro 32 version 5.1 MCA software one can be stored and analyzed in again as many times for further data processing.

It is often sufficient to establish a relative efficiency calibration using nuclides with two or more gamma rays with well-known relative intensity ratio. At present, the standard ^{22}Na , ^{60}Co , ^{137}Cs and ^{152}Eu gamma thin foil sources which were provided by IAEA and manufactured by Reactor Experiments Inc, California was measured with the reproducible geometry. Standard sources were placed vertically 1cm away from the HPGe detector, which is the same place as the sample position for calibration and efficiency determination and acquired for 900s to get good statistics. The calibration curve can be seen in Fig. 2.2. The recommended nuclear data of standard source used in calibration and efficiency determination are listed in Table 2.2.

The efficiency can be measured by using the following expression:

$$\varepsilon = \frac{PA}{\eta \int_{t_c}^{t+t_c} Q dt} , \quad Q = Q_0 e^{-\lambda t}$$

where, ε = efficiency

PA = number of counts under the photopeak

η = branching ratio

t = counting time

t_c = cooling time (reference date to starting time of measurement)

Q_0 = activity of the standard source at reference date

Q = activity of the standard source

The experimental determination of energy resolution is based on a measured of the Full Width at Half Maximum (FWHM) of a gamma ray peak at a specific energy. Logarithm scale of efficiency verses energy graph has been drawn by using the measured data to determine the efficiency at which would be used in data analysis. The efficiency graph is shown in Fig. 2.3.

(ii) Determination of Detector Efficiency

The electronic set-up for gamma counting system is shown in Fig. 2.1. It is often sufficient to establish a relative efficiency calibration and energy calibration using nuclides with two or more γ - rays with well known relative intensity ratios. At present, the standard gamma source ^{22}Na , ^{137}Cs and ^{60}Co , which were provided by IAEA and manufactured by Reactor Experiments Inc, California was measured with the reproducible geometry. It was placed vertically 3cm away the NaI (TI) crystal and acquired for 100 s to get a good statistics. The energy calibration curve is shown in Fig. 2.2.

Four photo peak were identified and full energy peak efficiencies were calculated from

$$\eta = \frac{PA}{I} \times 100 \%$$

where, PA = peak area of the photopeak

η = efficiency of the photopeak (%)

I = intensity of present time (kBq)

For ^{62}Cu sample, the geometrical efficiency (η) of the 3" x 3" NaI (TI) detector at the distance 3.0 cm from the NaI(Tl) crystal to the sample is found to be $\sim 7.2\%$ by using Fig. 2.3.

(iv) Neutron flux monitor

A spherical neutron dosimeter is used to monitor the neutron flux for each irradiation. This detector consists of 4mm x 8mm Li(Eu) scintillator surrounded by a 8" diameter sphere of polyethylene.

Table 2.2 Recommended Nuclear Data for Standard sources

Radio-nuclide	Half-life (d)	Photon Energy (keV)	Percentage per disintegration	Activity(Q_0) (kBq)
^{22}Na	950.34 \pm 0.13	511.006 \pm 0.002		431.6
		1274.54 \pm 0.02	99.94 \pm 0.02	
^{60}Co	1925.2 \pm 0.4	1173.238 \pm 0.004	99.87 \pm 0.06	362.2
		1332.501 \pm 0.005	99.98 \pm 0.009	
^{137}Cs	11009 \pm 11	661.665 \pm 0.009	84.60 \pm 0.5	392.6
^{152}Eu	4931 \pm 15	121.779 \pm 0.033	28.37 \pm 0.24	404.2
		244.639 \pm 0.005	7.51 \pm 0.06	
		344.272 \pm 0.007	26.58 \pm 0.18	
		411.111 \pm 0.011	2.234 \pm 0.013	
		443.979 \pm 0.01	3.121 \pm 0.018	
		778.89 \pm 0.016	12.96 \pm 0.07	
		867.38 \pm 0.03	4.16 \pm 0.06	
		964.05 \pm 0.03	14.62 \pm 0.06	
		185.83 \pm 0.03	10.16 \pm 0.05	
		1112.08 \pm 0.04	13.56 \pm 0.06	
	1208.0 \pm 0.03	20.58 \pm 0.09		

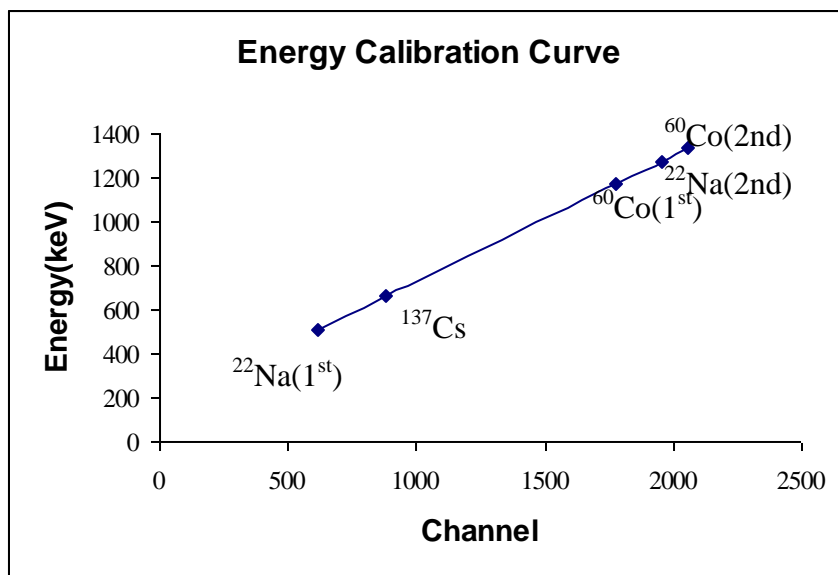


Fig. 2.2 Energy calibration curve

source	channel	Energy(keV)
^{22}Na 1 st peak	615	511
^{137}Cs peak	880	661
^{60}Co 1 st peak	1778	1173
^{22}Na 2 nd peak	1956	1274
^{60}Co 2 nd peak	2058	1332

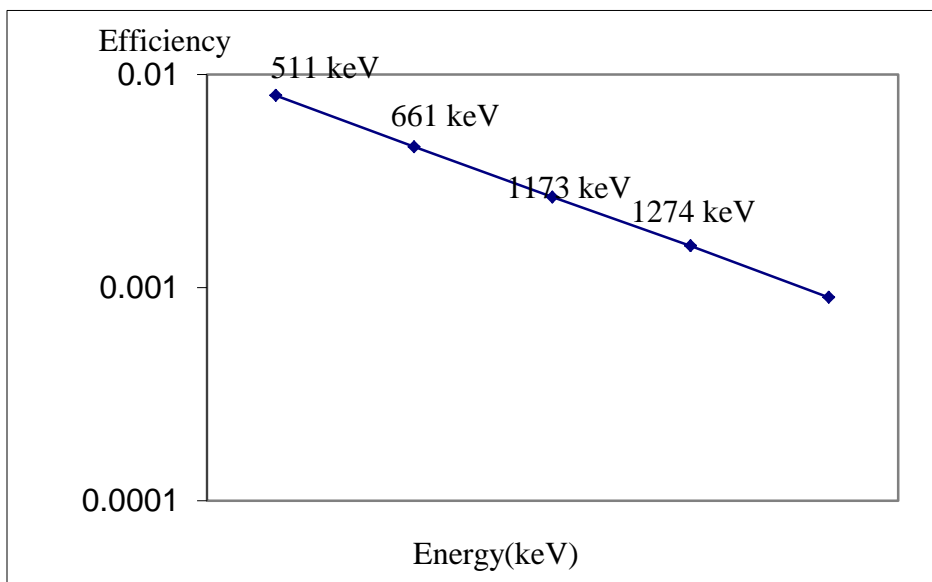


Fig. 2.3 Energy efficiency curve

Energy(keV)	Efficiency
511	0.00797
661	0.00458
1173	0.00266
1274	0.00157
1332	0.0009

2.3.2 Experimental Procedure

2.3.2.1 Sample Preparation

In this case, chemical compounds containing the element of interest were selected on the basis of matrix sensitivity to 3 MeV and 14 MeV neutrons. Sample were packed uniformly and pressed to pellet with 2 ton pressure by Hydraulic press, SPECAC, Cambridge Electric Industries.. To get accurate neutron flux spectroscopy pure circular shaped copper foils samples of 2.5 cm in diameter are used. The pallet was weighted with Sartorius, MC1, Science balance. The weight of each foil is 1.5 g and the diameter of each is 2.5 cm.

2.3.2.2 Sample Irradiation

For the activation process, irradiation time selected was governed by the half-life of the induced activity and abundance of the isotope of interest in the target element. The environmental background is subtracted from all spectra and the samples generally were counted for time period depends on their irradiation time. Irradiations were carried out by using Multivolt (NA 150-04) Pump Type Neutron Generator and Pu-Be isotropic source which produced neutrons with 14 MeV and 3 MeV respectively. Thus, one chose 30 min for each reaction, in which two samples were irradiated simultaneously on for to calculate specific activity and element content and another for flux monitoring.

2.3.2.3 Neutron flux determination

For the absolute flux measurements, the foils activation technique was used. The flux of neutron sources can be expressed as a function of operational parameters of the techniques in the following manner:

$$\phi = \frac{A(t_i)}{n \sigma E A \eta (1 - e^{-\lambda t_i}) (e^{-\lambda t_{c1}} - e^{-\lambda t_{c2}})}$$

where, ϕ = neutron flux (n cm⁻² s⁻¹)

n = number of molecules

σ = reaction cross section (barn)

λ = disintegration constant

η = branching intensity of gamma rays

E= detector efficiency

A= natural abundance

t_i = irradiation time

t_{c1} = initial cooling time (or) decay time

t_{c2} = end cooling time (or) decay time

and then, one may obtain neutron flux distribution or neutron field from

$$F = \phi \times t_i \text{ (n cm}^{-2}\text{)}$$

2.3.2.4 Determination for Cross-section of Na

Studies on nuclear reactions enhanced our understanding of basic nuclear theory and useful information for practical application in several fields. Knowledge of the threshold reactions, especially the (n,p), (n, α) and (n,2n) reactions are of practical importance in the field of fast reactions analysis. Neutron activation concerned with radiation damage, radiation shielding in fusion reactor design as well as induced activity, neutron dosimetry, nuclear transmutation and so on.

In order to measure fast neutron fluxes by activation techniques, there are several useful neutron reactions, which results in a radioactive product. There are (n, γ), (n,p), (n,2n), (n,d), (n, α) and (n,f) reactions. The radio activation method is best studied to measure the neutron cross section. The key to radio activation method of determining neutron flux is to select a detector whose half-life gives sufficient proof that the particular reaction sought occurs.

The choice of detector will be generally determined which technique to use for a flux determination. Activation technique is based on the irradiation of a chosen sample foil by neutrons and lead to radioactive residual nucleus. The activities produced by this residual nucleus are measured by absolute beta or gamma counting.

In this research (n, α) and (n,2n) reaction are used for the cross section and flux calculation for Na contain monosodium glutamate sample. The following expression can be used to obtain the cross section data.

$$\sigma = \frac{A(t_i)}{n \phi E A \eta (1 - e^{-\lambda t_i}) (e^{-\lambda t_{c1}} - e^{-\lambda t_{c2}})}$$

where, ϕ = neutron flux (n cm⁻² s⁻¹)

n = number of molecules

σ = reaction cross section (barn)

λ = disintegration constant

η = branching intensity of gamma rays

E = detector efficiency

A = natural abundance

t_i = irradiation time

t_{c1} = initial cooling time (or) decay time

t_{c2} = end cooling time (or) decay time

2.3.2.5 Determination of linear absorption coefficient for Na

In their passage through matter the gamma-ray photons are absorbed so that the intensity falls off in an exponential manner. This arises from the fact that the extent of, absorption in a small thickness dx of matter, at any point in the medium is proportional to the radiation intensity at that point and to the thickness traversed, .ie,

$$dI = -\mu I dx \quad \text{or} \quad \frac{dI}{I} = -\mu dx$$

where I is the intensity expressed as photons (or MeV) per cm² per sec, and the proportionality constant, μ , usually given in cm⁻¹ units, is called the linear absorption coefficient of the absorber for the given radiation. If a collimated beam of monoenergetic gamma rays of intensity I_0 passes through a thickness x cm of absorber, the intensity I_x of the emergent beam is obtained as follows:

$$I_x = I_0 e^{-\mu x}$$

In Table 2.3 data of absorption coefficient for Na are shown and in Fig 2.4 the general character of the variation of the radiation intensity with thickness of the absorber which is total linear gamma rays absorption coefficient curve can be seen.

2.3.2.6 Calculation of Experimental Sensitivity

The calculated sensitivity was corrected for both neutron and gamma rays attenuation for every sample using the relationship.

$$L = \frac{S}{e^{-\Sigma y} e^{-\mu x}}$$

where, L = corrected sensitivity

S = uncorrected

Σ = total microscopic cross section

y = effective sample thickness neutron attenuation in sample

μ = total linear gamma rays absorption coefficient

x = effective sample thickness for gamma rays attenuation sample

Table 2.3 Data for absorption coefficient of Na

Distance (cm)	Net area (Counts)	Net Count rate (cps)	Ratio
0	178828 ± 620	2947.07	1.0000
0.25	161496 ± 638	2671.12	0.9004
0.50	153482 ± 615	2547.64	0.8645
0.75	144339 ± 650	2347.84	0.8019
1.00	134073 ± 620	2232.32	0.7575
1.25	123864 ± 628	2062.34	0.6998
1.50	116453 ± 611	1945.42	0.6601
1.75	107657 ± 626	1797.28	0.6097
2.00	103395 ± 614	1714.68	0.5818
2.25	97829 ± 529	1627.77	0.5533

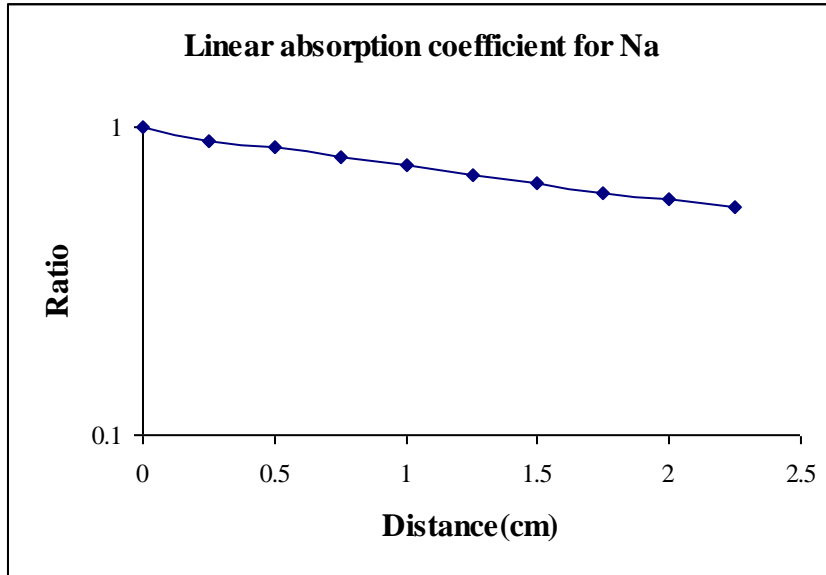


Fig 2.4 Total Linear Absorption Coefficient Curve for Sodium

2.4 Results and Discussion

2.4.1 Results

(i) Cross section data for MSG (Monosodium Glutamate) sample

Monosodium Glutamate sample contains Sodium element about 13%. Sodium occurs naturally as one isotope of mass 23. This isotope has excellent cross sections for reactions with both thermal and fast neutrons and can be readily measured neutron activation techniques.

Activation analysis of sodium has some advantages over alternate methods for sodium determination. While sodium has good spectroscopic characteristics for its determination by flame photometry or atomic absorption, microlevels of sodium are difficult to determine directly using other instrumental methods of analysis or wet chemical techniques. The solution chemistry of sodium is very limited. Sodium does not undergo good gravimetric or complex metric reactions which can be employed for its determination. On the other hand, atomic absorption provides an excellent approach to the determination of microamounts of sodium in aqueous or nonaqueous media.

The most sensitive reaction for the determination of sodium is the (n,α) reaction, which produces ^{20}F . It can be showed that as little as 1mg of sodium could be measured with good precision (10%) using this technique. Fluorine was also noted to interfere. The irradiation and counting conditions for this analysis are such Compton continuum from oxygen in the sample falls under 1.63MeV peak. It can be also used a sample baseline technique to correct for any contributions from high energy peaks.

A 14 MeV neutron generator is used to irradiate the patient: sufficient thermalization of the flux occurs due to body water as well as from some added polyethylene shielding to provide the usable thermal flux. Exposures in the range of 0.05 rad were used and the patient was then subjected to whole-body counting. The results from these experiments indicate that the technique provides whole-body sodium figures that are in good agreement with those from previous isotope dilution techniques.

In this study, we obtained the cross section data of $^{23}\text{Na}(n,\alpha)^{20}\text{F}$ reaction for the incident 14MeV neutron by Neutron Activation Analysis (NAA). The measured spectrum for

(n,2n) and (n, α) reactions are shown in Fig 2.5 and Fig2.6. The parameters for the measured reaction are calculated and described in Table 2.4.

In the present experiment, sodium contain Monosodium Glutamate is used to measure the total reaction cross section measurement. The measured total cross section of $^{23}\text{Na}(n,\alpha)^{20}\text{F}$ is very well agree with the evaluated nuclear data of JENDL-FF and SCINCROS II calculation and other data of SS-Nargolwalla within error bars. The comparison among the measured data and evaluated nuclear data of JENDL-FF and SCINCROS II and other data can be seen in Table 2.5 and Fig 2.7.

(ii) Data for Sodium Content

In this research, one estimated first the flux distribution of all neutron sources, neutron generator and isotopic Pu-Be sources. In Fig 2.8 to Fig 2.10, one shows the spectrum of MSG (Monosodium Glutamate), NaCl and Na_2CO_3 samples.

The associated nuclear data and counting data are given in Table 2.6 and 2.7. Information regarding sample identify and size relevant activation and nuclear data has also been included. In Table 1.4, the comparison of experimental observation with actual element content of chemical compound, sodium chloride NaCl, Monosodium glutamate $\text{C}_5\text{H}_8\text{NNaO}_4\text{H}_2\text{O}$ and sodium carbonate Na_2CO_3 , are shown. The experimental data are comparable within the $\pm 10\%$ errors. By using Table 2.8, we can draw the comparison graph of Na contents percentage for Ucorrected, Corrected and Actual in Fig 2.11.

After the correction, the sensitivity of uncorrected sample attenuation may be changed 10 to 50, the practical analysis of content of chemical compound may be closed to the actuated content.

2.4.2 Discussion

In view of many approximations made in this study, and bearing in mind the fundamental purpose of this work as outlined in the introduction, no attempt was made to evaluate the accuracy of the calculated sensitivity. As estimate of $\pm 10\%$ would, however, not be unreasonable.

Table 2.4 Parameters of Measured Reactions

Sr	Sample	Nuclear Reaction	Q value (MeV)	Threshold Energy (MeV)	Half-life $T_{1/2}$ (min)	Emission γ Energy (MeV)	Emission Rate (%)
1	^{63}Cu	$^{63}\text{Cu}(n,2n)^{62}\text{Cu}$	-10.8414	11.0152	9.74	0.511	196
2	^{23}Na	$^{23}\text{Na}(n,\alpha)^{20}\text{F}$	-3.7334	3.8973	0.19	1.368	100

Table 2.5 The comparison of total cross section of $^{23}\text{Na}(n,\alpha)$ the measured data, evaluated nuclear data(JENDL-FF and SCINCROS II calculations) and other data

Reaction	Neutron Energy (MeV)	Present σ (mb)	JENDL-FF σ (mb)	SCINCROS II σ (mb)	SS-Nargolwalla σ (mb)
$^{23}\text{Na}(n,\alpha)^{20}\text{F}$	14.7	226.05±18.15	217.45	210.57	222.00

Table 2.6 Sample Data

Element Sodium
 Sample Monosodium Glutemate $C_5H_8NNaO_4H_2O$
 Sodiumchloride NaCl
 Sodium carbonate Na_2CO_3

code	Sample	Element	Sample Wt	Element Wt	Neutron Flux
1	MSG	Na	1.5	0.18449	1.1706×10^6
2	MSG	Na	10.43	1.2828	2.162×10^5
3	MSG	Na	182.3449	22.4267	2.224×10^5
4	NaCl	Na	121.63	48.2326	2.242×10^5
5	MSG	Na	392.165	48.2339	2.164×10^5
6	Na_2CO_3	Na	9.98	2.16	2.205×10^5

Table 2.7 Experimental sensitivity

Sr	Net Counts	Activity cps	Experimental Sensitivity (Net Counts/g)							
			Uncorrected				Corrected (%)			
			Sample	Element	Sample	Element	Sample	Element	Sample	Element
					μ_1	μ_2	μ_3	μ_1	μ_2	μ_3
1	42.00	0.02	28.0000	227.653	19.3	8.9	21.5	19.3	8.9	21.5
2	11.465	1.91	1099.2333	8937.481	20.7	21.3	17.7	20.7	21.3	17.7
3	111898	13.81	613.6613	4989.499	16.7	20.2	22.7	16.7	20.2	22.7
4	93862	11.59	771.7011	1946.028	16.6	19.1	27.7	16.6	19.1	27.7
5	117886	14.55	300.6031	2444.049	20.9	23.7	23.7	20.9	23.7	23.7
6	76586	4.08	300.6031	2444.049	20.9	23.7	23.7	20.9	23.7	23.7

Table 2.8 The comparison of experimental observation with actual elemental content of chemical compound, Sodium chloride NaCl, Monosodium glutamate $C_5H_8NNaO_4H_2O$ and Sodium carbonate Na_2CO_3

Sr	Sample	Weight (g)	Content of Na	Net Content	Percentage (%)		
					Uncorrected	Corrected	Actual
1	NaCl	121.63	48.23	11.59	35.356	38.89	39.65
2	MSG	392.165	45.23	14.55	13.761	12.385	12.29
3	Na_2CO_3	9.98	2.16	4.94	21.690	21.69	21.69

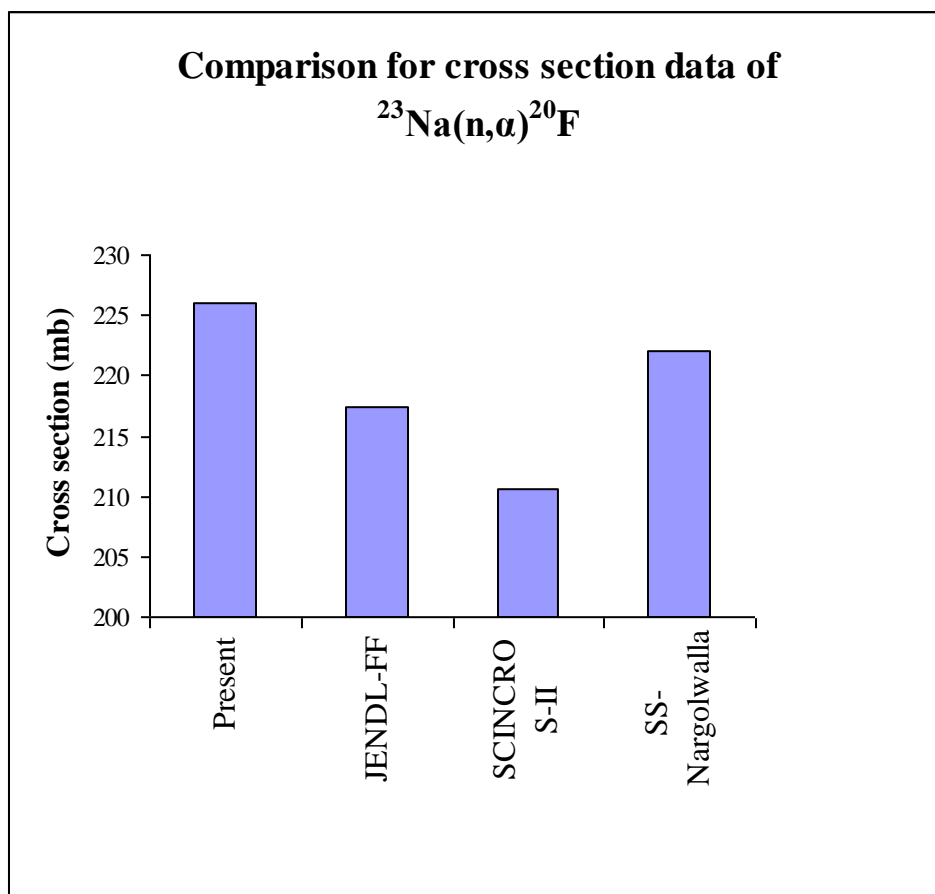


Fig. 2.7 The comparison of total cross-section of $^{23}\text{Na}(n, \alpha)$ the measured data, evaluated nuclear data of JENDL-FF and SCINCROS II calculation and SS Nargolwalla

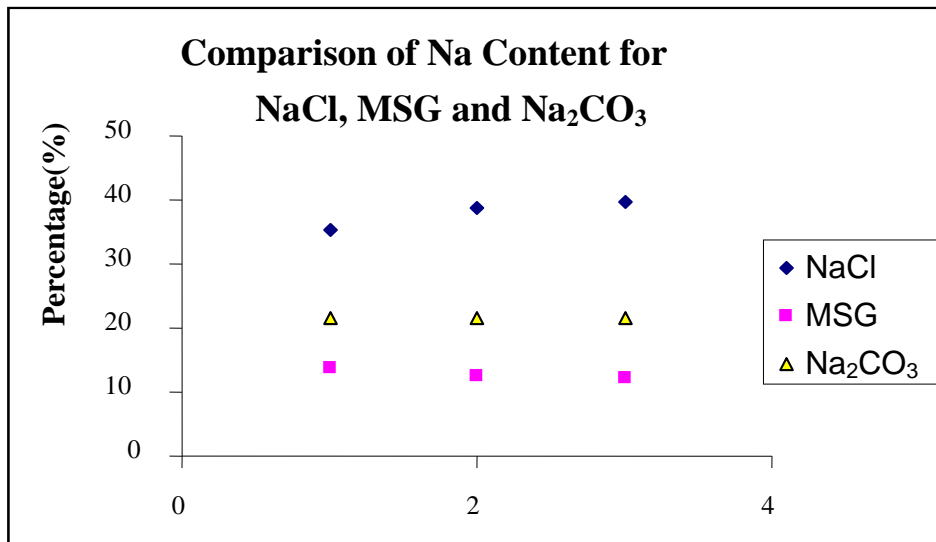
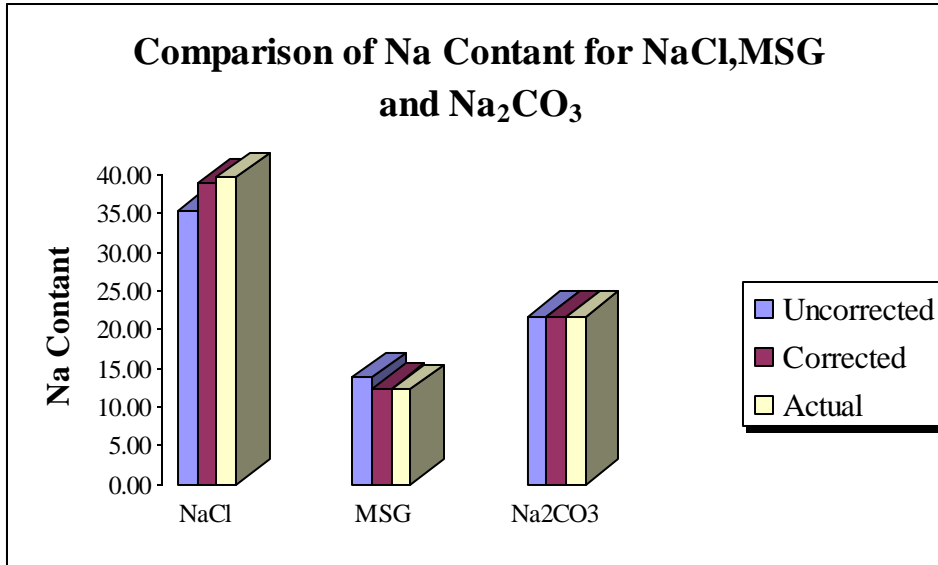


Fig.2.11 Comparison of Na contents percentage for Uncorrected, Corrected and Actual data

CHAPTER III

ANALYSIS OF THE EDXRF METHOD

3.1 Introduction

In this section, all the experimental procedures are involved for the present work. The analyzed samples was monosodium glutamate (MSG). The concentration of elements contained in this sample was determined by EDXRF method. There studied on the relationship between the elements contained in these samples of interest and quality of these one.

When a primary x-ray excitation source from an x-ray tube or a radioactive source strikes a sample, the x-ray can either be absorbed by the atom or scattered through the material. The process in which an x-ray is absorbed by the atom by transferring all of its energy to an innermost electron is called the "photoelectric effect." During this process, if the primary x-ray had sufficient energy, electrons are ejected from the inner shells, creating vacancies. These vacancies present an unstable condition for the atom. As the atom returns to its stable condition, electrons from the outer shells are transferred to the inner shells and in the process give off a characteristic x-ray whose energy is the difference between the two binding energies of the corresponding shells. Because each element has a unique set of energy levels, each element produces x-rays at a unique set of energies, allowing one to non-destructively measure the elemental composition of a sample. The process of emissions of characteristic x-rays is called "X-ray Fluorescence," or XRF. Analysis using x-ray fluorescence is called "X-ray Fluorescence Spectroscopy." In most cases the innermost K and L shells are involved in XRF detection. A typical x-ray spectrum from an irradiated sample will display multiple peaks of different intensities.

The characteristic x-rays are labeled as K, L, M or N to denote the shells they originated from. Another designation alpha (α), beta (β) or gamma (γ) is made to mark the x-rays that originated from the transitions of electrons from higher shells. Hence, a K_{α} x-ray is produced from a transition of an electron from the L to the K shell, and a K_{β} x-ray is

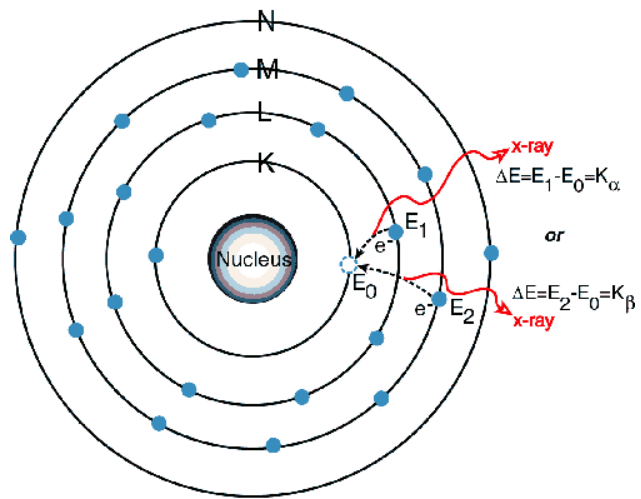
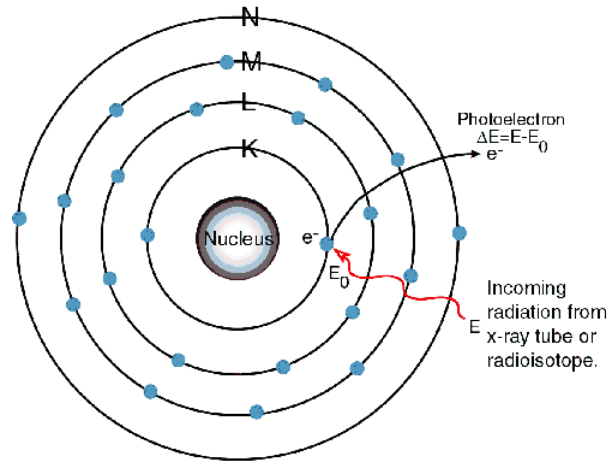
produced from a transition of an electron from the M to a K shell, etc. Since within the shells there are multiple orbits of higher and lower binding energy electrons, a further designation is made as α_1 , α_2 or β_1 , β_2 , etc. to denote transitions of electrons from these orbits into the same lower shell.

The XRF method is widely used to measure the elemental composition of materials. Since this method is fast and non-destructive to the sample, it is the method of choice for field applications and industrial production for control of materials. Depending on the application, XRF can be produced by using not only x-rays but also other primary excitation sources like alpha particles, protons or high energy electron beams.

Sometimes, as the atom returns to its stable condition, instead of emitting a characteristic x-ray it transfers the excitation energy directly to one of the outer electrons, causing it to be ejected from the atom. The ejected electron is called an "Auger" electron. This process is a competing process to XRF. Auger electrons are more probable in the low Z elements than in the high Z elements.

- 1) An electron in the K shell is ejected from the atom by an external primary excitation x-ray, creating a vacancy.
- 2) An electron from the L or M shell "jumps in" to fill the vacancy. In the process, it emits a characteristic x-ray unique to this element and in turn, produces a vacancy in the L or M shell.
- 3) When a vacancy is created in the L shell by either the primary excitation x-ray or by the previous event, an electron from the M or N shell "jumps in" to occupy the vacancy. In this process, it emits a characteristic x-ray unique to this element and in turn, produces a vacancy in the M or N shell.

The excitation energy from the inner atom is transferred to one of the outer electrons causing it to be ejected from the atom.



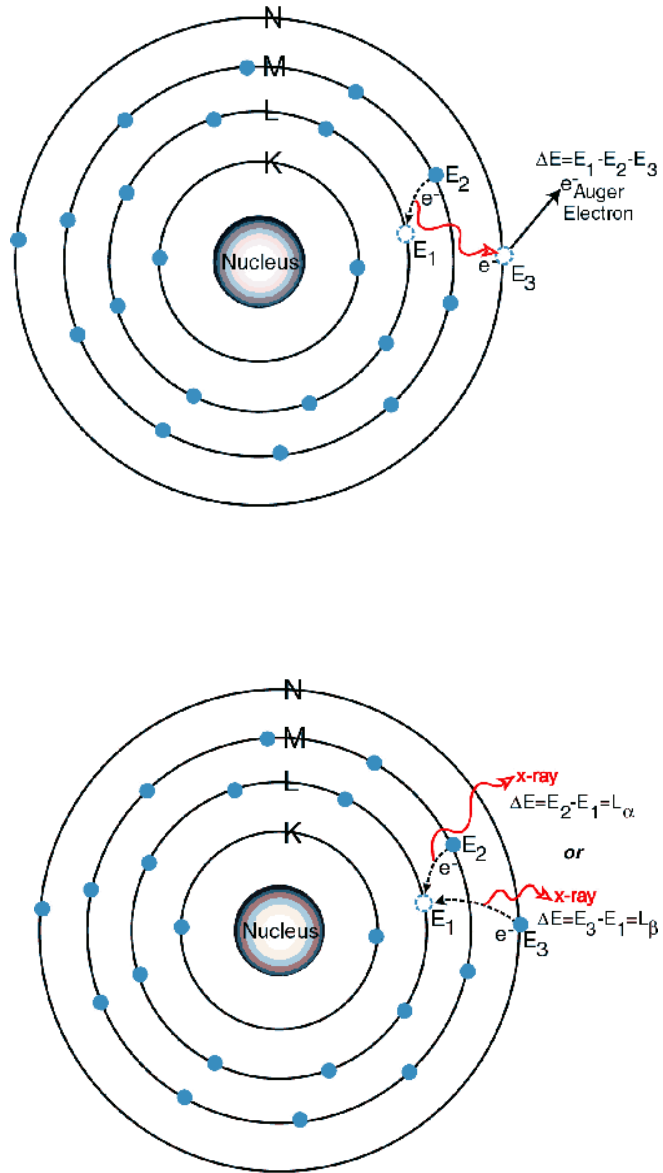


Fig 3.1 X-Ray Fluorescence Process Example: Titanium Atom (Ti=22)

3.2 The Shimadzu EDX – 700 Spectrometer

The energy dispersive X-ray fluorescent spectrometer used through this investigation is a computer controlled SHIMAZU EDX-700 (Japan) spectrometer. The EDX-700 is an energy dispersive XRF system. X-rays fluorescence (XRF) uses X-ray to excite the MSG samples. The individual elements comprising the sample re-emit their own characteristic X-rays. The EDX-700 detects elements presented in the material. This indicates that the X-rays are detected using a lithium drifted silicon semiconductor. The detector can store at room temperature but the working temperature of detector must be that of liquid nitrogen (-170 °C). The EDX-700 spectrometer could not operate about the specific temperature.

The samples were placed in the sample holder which can be measured sixteen samples at one time. The samples were covered with cylindrical shape cover and they are pumped up to vacuum. This EDXRF design has a number of advantages. It is a compact size and easy operability over other types of XRF. Because of the shortest distance between the sample and the detector analysis is possible in the atmosphere.

Main Specifications of EDX-700

Method of measurement	:	Energy Dispersive X-ray Fluorescence Analysis
Sample type	:	Solid, liquid or powder
Element range	:	Na – U (EDX-700)
Sample size	:	300 mm (dia) x 150 (H) mm max

X-ray Generator

X-ray tube	:	Rh target
Tube voltage	:	5 – 50 kV
Tube current	:	1 – 1000 μ A
Cooling method	:	Air cooling (with a fan)
Exposure area:	:	10 mm dia (standard)
Primary filters	:	Automatic selection from among 5 types of filter

Detector

Type :	Si(Li) detector
LN ₂ supply :	Only during measurement
Dewar capacitor :	3 liters
LN ₂ consumption :	less than 1 liter/day
Detection area :	10 mm ²
Resolution :	< 155 eV (Mn-K α , 1500 cps)

MCA

Resolution :	2084 ch
Gain :	10 eV/ch and 20 eV/ch

Sample Chamber

Atmosphere in spectrometer :	Air, Vacuum, 'He'
Sample change :	8/16 sample turret

Data Processing Unit

Main unit :	IBM PC/AT compatible
Memory :	More than 32 MB
Operation system :	Windows® 95, 98 or Windows NT

Software

Qualitative analysis :	Software for measurement and analysis of measured data
Quantitative analysis :	Calibration curve method, matrix correction, FP method, background FP method
Matching software Utility (intensity content) :	Automatic correction functions (intensity correction, energy correction, full width of half maximum FWHM correction)

3.3 Analysis of EDXRF Method

MSG sample was made into fine powder and this sample was pressed into pellet with 2.5 cm in diameter. Then the weight of pellet was measured by using an electronic scientific balance.

The EDXRF machine (Shimadzu EDX-700) at Universities' Research Centre is used for determination of the trace elements in the sample of interest. The machine can provide the information of elements from sodium (Na) to uranium (U). The Shimadzu EDX-700 can automatically identify all elements in a sample based upon a library of X-ray data. In addition to this standard feature, quantitative information is also provided.

The X-ray tube was operated at 50 kV, 14 μ A (auto) in vacuum. The X-ray beam from rhodium (Rh) target, which was set to pass through the 10 mm collimator, was allowed to excite the sample for 100 second. The characteristic X-rays of each element contained in sample was detected by the Si(Li) detector.

The X-ray spectrum displayed on the monitor of computer was analyzed by using software with fundamental parameter (FP) method. The fundamental parameter (FP) method of analysis is very useful for determination of elemental analysis.

For safety, we need to know how this MSG can be harmful for the health the users. Therefore, we have to analyze the toxic elements in MSG. It was analyzed by EDXRF method in this work. The EDXRF technique is a multi-elemental quantitative determination and it can provide concentrations of many elements contained in the sample by single experiment.

3.4 Experimental Set-up

In this research, the concentrations of elemental compounds contained in the MSG sample was measured using the Shimadzu Energy Dispersive X-ray Spectrometer (EDX-700 System) at Universities' Research Centre (URC), Yangon University. This system is a compact in high performance EDXRF analyzer. Instrumental control system and data

analysis system are performed by a personal computer (PC) that is connected to the EDXRF system. The experimental set-up of EDX-700 system is shown in Fig 3.2.

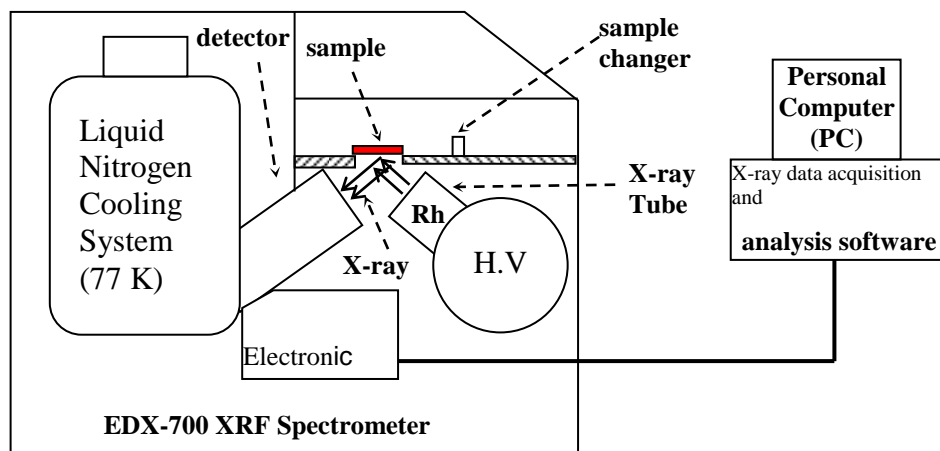


Fig 3.2 Experimental set-up of EDXRF system

The EDX-700 system is composed of two parts: the x-ray spectrometer and personal computer (PC). The spectrometer contains: the x-ray generating elements; x-ray tube (Rh), sample chamber, Si(Li) detector, detector electronics, microprocessor controller, liquid nitrogen (LN₂) cooling system and associated power supplies. The personal computer (PC) includes the data memory board and other standard PC elements. The collected spectra were analyzed using the EDX-700 Qualitative and Quantitative Analysis software. The Fundamental Parameter (FP) method was used for elemental analysis.

By the nature of EDXRF experiment, the sample must be in the form of pellet. First, the samples were made into fine powder using grinding machine and then a palette using hydraulic press. The x-rays from the Rh target are used for the excitation of the sample. The characteristic x-rays from each element contained in the sample are detected by the Si(Li) detection system. Then the x-ray spectrum is analyzed with the help of the personal computer to obtain the concentration of each element in the sample.

3.5 Results And Discussion

The EDXRF machine (Shimadzu EDX-700) is used for determination of the elements in the sample of interest. The machine can provide the information of elements from sodium (Na) to uranium (U). The EDX-700 can automatically identify all elements in a sample based upon a library of X-ray data. In addition to this standard feature, quantitative information is also provided.

The X-ray spectrum displayed on the monitor of computer was analyzed by using software with fundamental parameter (FP) method. The fundamental parameter (FP) method of analysis is very useful for determination of elemental analysis.

In this study, monosodium glutamate was analyzed using the EDX-700 spectrometer. The concentration of elemental compounds contained in this sample is 100 % sodium (Na). Fig 3.3 shows the result of concentrations of elemental compounds in comparison. According to the results, it was found that the major element in the monosodium glutamate sample of interest is sodium (Na) as shown in Fig 3.3.

3.6 Conclusion

In this study, the quantitative data are calculated by the EDX-700 software, which is used the calibration system with the internal standards. These data are obtained on the 100 percent of weightiness of just inorganic elements contained in the sample of interest and not considered on the organic compounds and dark matrix elements. It means that the data show the relative concentrations of elements contained in the samples of analysis. The mechanical stability of EDXRF spectrometer and the optimization of the excitation source lead to the versatile applications. The software available permits the quantitative determination of the elements within a short time without the need for complicated sample preparation procedures.

According to the results, it was found that the major element is sodium only. But, the elements of sulphur (S), strontium (Sr), mercury (Hg), lead (Pb), arsenic (As) and

scandium (Sc), which are known as toxic elements, were not found in this sample. Therefore, the above sodium glutamate is assumed to be safe in use.

CHAPTER IV

X RAYS DIFFRACTION AND CRYSTALLOGRAPHY

4.1 X-Ray Diffraction Technique (XRD)

X-ray diffraction method which has been developed rapidly in recent years. X-ray diffraction technique (XRD) is a powerful technique for determination of crystal structure, interplanar spacing by using x-ray beam. It provides simple and nondestructive information on the nature of intermetallic and crystalline phase usually in a very short time of period. In addition, the technique can be used to obtain information on grain size, texture of grains crystal defect densities XRD, a beam of X-ray directed on a crystalline material may experience diffraction (constructive interference) as a result of its interaction with a series of parallel atomic planes according to Bragg's law. Since interplanar spacing is a function of the miller indices, lattice parameters and the crystal structure, XRD technique is capable of gathering many useful information relating the crystal structures.

4.2 Basic Principles of XRD

X-ray is a form of electromagnetic radiation with higher energy and shorter wavelength ($\sim 0.1\text{nm}$) as compared with those of light of wavelength (400~800nm). It is produced when a target metal is bombarded by high-energy electron which is accelerated across a vacuum tube under high electrical field. The radiation emitted during the bombardment consists of both white radiation and characteristic radiation.

Characteristic radiation will be excited only when a certain voltage is exceeded, since sufficient energy must be provided to eject one of the inner shell electrons. The vacancy produced is then filled up by another electron from higher energy levels. If the electron is fallen from an adjacent shell (L-shell), the radiation emitted is known as K_{α} characteristic

radiation; if the K-shell vacancy is filled by an electron from M-shell, then K_{β} characteristic radiation is produced.

If an x-ray strikes an atom, it will be weakly scattered in all directions. If it encounters a periodic array of atoms, the waves scattered by each atom will reinforce in certain directions and cancel in others. Geometrically, one may imagine that a crystal is made up of families of lattice planes and that the scattering from a given family of planes will only be strong if the x-rays reflected by each plane arrive at the detector in phase.

In XRD, a beam of X-ray directed on a crystalline material may experience diffraction (constructive interference) as a result of its interaction with a series of parallel atomic planes according to Bragg's law is shown in Fig. 4.1. Bragg's law is given by,

$$n\lambda = 2d_{hkl}\sin\theta \quad (4.1)$$

If Bragg's law is not satisfied, the condition for constructive interference cannot be fulfilled. As a result, a very low intensity (destructive interference) diffracted beam can be observed. According to Bragg's law, it can be shown that the most widely spaced lattice planes (with largest d value) will give rise to a refraction at the smallest Bragg's angle, θ .

The value of interplanar spacing, d_{hkl} is a function of miller indices (h,k and l) as well as the lattice parameter. For crystal structures having cubic symmetry,

$$d_{hkl} = \frac{a}{\sqrt{h^2 + k^2 + l^2}} \quad (4.2)$$

The planes of the family (hkl) are equidistant among each other, and the interplanar spacing decreases with increasing miller indices (hkl).

Due to extra atoms which are not situated at the lattice sites, for example, atoms located at center of unit cell for BCC structure and atoms located at face center for FCC structure ; the extra atoms will act as extra scattering centers which can produce out-of-plane scattering at certain Bragg's angles. Hence for BCC crystal structure, only planes

with $h+k+l$ equal to even number is permitted and for FCC crystal structure, all of h, k and l must be either odd or even number for diffraction to occur.

The geometry of diffraction in a single grain is described through the reciprocal lattice. If the crystal lattice is defined by three vectors \mathbf{a} , \mathbf{b} , and \mathbf{c} , there are three reciprocal lattice vectors defined as

$$\mathbf{a}^* = \frac{2\pi \mathbf{b} \times \mathbf{c}}{\mathbf{a} \cdot \mathbf{b} \times \mathbf{c}} \quad (4.3)$$

and cyclic permutations thereof for \mathbf{b}^* and \mathbf{c}^* (in the chemistry literature the factor 2π is usually eliminated in this definition). These vectors define the reciprocal lattice, with the significance that any three integers (hkl) define a family of lattice planes with spacing $d = 2\pi / |\mathbf{h}\mathbf{a}^* + \mathbf{k}\mathbf{b}^* + \mathbf{l}\mathbf{c}^*|$, so that the diffraction vector $\mathbf{K} = \mathbf{h}\mathbf{a}^* + \mathbf{k}\mathbf{b}^* + \mathbf{l}\mathbf{c}^*$ satisfies $|\mathbf{K}| = 2\pi/d = 4\pi \sin \theta / \lambda$ (most chemists and some physicists define $|\mathbf{K}| = 1/d = 2 \sin \theta / \lambda$).

The intensity of the diffracted beam is governed by the unit cell structure factor, defined as

$$F_{hkl} = \sum_j e^{i\mathbf{K} \cdot \mathbf{R}_j} f_j e^{-2W} \quad (4.4)$$

where \mathbf{R}_j is the position of the j^{th} atom in the unit cell, the summation is taken over all atoms in the unit cell, and f_j is the atomic scattering factor, tabulated in, e.g., the International Tables for Crystallography and is equal to the number of atomic electrons at $2\theta = 0$, decreasing as a smooth function of $\sin \theta / \lambda$ (there are “anomalous” corrections to this amplitude if the x-ray energy is close to a transition in a target atom). The Debye-Waller factor $2W$ is given by $2W = \mathbf{K}^2 u_{\text{rms}}^2 / 3$, where u_{rms} is the (three-dimensional) root-mean-square deviation of the atom from its lattice position due to thermal and zero-point fluctuations. Experimental results are often quoted as the thermal parameter B , defined as $8\pi u_{\text{rms}}^2 / 3$, so that the Debye-Waller factor is given by $2W = 2B \sin^2 \theta / \lambda^2$. Note that thermal fluctuations of the atoms about their average position weaken the diffraction lines but do not broaden them. As long as the diffraction is sufficiently weak (kinematics limit, assumed valid for most powders), the diffracted intensity is proportional to the square of

the structure factor. In powder diffraction, it is always useful to bear in mind that the positions of the observed peaks indicate the geometry of the lattice, both its dimensions and any internal symmetries, whereas the intensities are governed by the arrangement of atoms within the unit cell. In a powder experiment, various factors act to spread the intensity over a finite range of the diffraction angle, and so it is useful to consider the integrated intensity (power) of a given peak over the diffraction angle,

$$P_{hkl} = \left[\frac{P_0 \lambda^3 R_e^2 l V_s}{16\pi R V^2} \right] M_{hkl} F_{hkl}^2 \left(\frac{1 + \cos^2 2\theta}{\sin 2\theta \sin \theta} \right) \quad (4.5)$$

where P_0 is the power density of the incident beam, $R_e = 2.82$ fm is the classical electron radius, l and R are the width of the receiving slit and the distance between it and the sample, and V_s and V are the effective illuminated volume of the sample and the volume of one unit cell. The term M_{hkl} is the multiplicity of the hkl peak, e.g., 8 for a cubic hhh and 6 for a cubic $h00$, and $(1 + \cos^2 2\theta)/(\sin \theta \sin 2\theta)$ is called the Lorentz polarization factor. The numerator takes the given form only for unpolarized incident radiation and in the absence of any other polarization-sensitive optical elements; it must be adapted, e.g., for a synchrotron-radiation source or a diffracted-beam monochromator. There are considerable experimental difficulties with measuring the absolute intensity either of the incident or the diffracted beam, and so the terms in the square brackets are usually lumped into a normalization factor, and one considers the relative intensity of different diffraction peaks, or more generally, the spectrum of intensity vs. scattering angle.

There are two major problems in using powder diffraction measurements to determine the atomic structure of a material. First, as noted above, peaks overlap, so that the measured intensity cannot be uniquely assigned to the correct Miller indices (hkl). Second, even if the intensities were perfectly separated so that the magnitudes of the structure factors were known, one could not Fourier transform the measured structure factors to learn the atomic positions because their phases are not known.

4.2.1 Types of XRD Techniques

In X-ray diffraction studies, the probability that the atomic planes with right orientations are exposed to X-rays is increased by adopting one of the following methods:

- (i) the laue's technique
- (ii) the rotating crystal method
- (iii) the powder method

	λ	θ
(i) Laue's method	Variable	Fixed
(ii) Rotating –Crystal method	Fixed	Variable (in part)
(iii) Powder method	Fixed	Variable

which are carried out by either varying the Bragg's angle or the X-ray wavelength values.

1. The Laue method

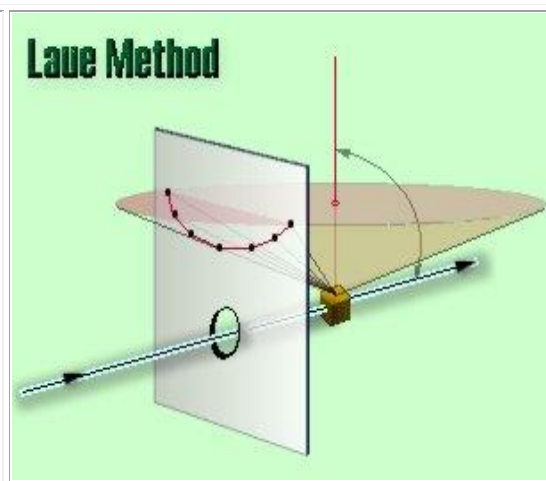
In this method, a stationary single crystal is bombarded with an X-ray beam of varying wavelength. The Laue method is capable of indicating the symmetry of crystal and can be used to determine the orientation of single crystal.

A single crystal is held stationary and a beam of white radiations is inclined on it at a fixed glancing angle θ , i.e., θ is fixed while λ varies. Different wavelengths present in the white radiations select the appropriate reflecting planes out of the numerous present in the crystal such that the Bragg's condition is satisfied. This technique is called the Laue's technique.

Back-reflection Laue

In the back-reflection method, the film is placed **between** the x-ray source and the crystal. The beams which are diffracted in a backward direction are recorded.

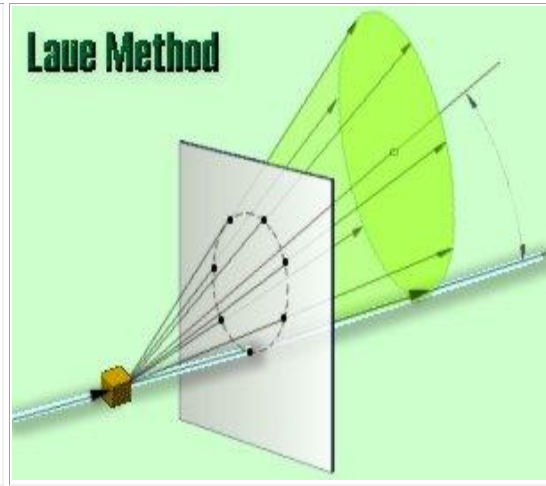
One side of the cone of Laue reflections is defined by the transmitted beam. The film intersects the cone, with the diffraction spots generally lying on an hyperbola.



Transmission Laue

In the transmission Laue method, the film is placed **behind** the crystal to record beams which are transmitted through the crystal.

One side of the cone of Laue reflections is defined by the transmitted beam. The film intersects the cone, with the diffraction spots generally lying on an ellipse.



Crystal orientation is determined from the position of the spots. Each spot can be indexed, i.e. attributed to a particular plane, using special charts. The Greninger chart is used for back-reflection patterns and the Leonhardt chart for transmission patterns.

The Laue technique can also be used to assess crystal perfection from the size and shape of the spots. If the crystal has been bent or twisted in anyway, the spots become distorted and smeared out.

2. The rotating crystal method

The method utilizes a single crystal rotating in a beam of fixed wavelength X-ray. This technique is employed in this project for determining of crystal structure changes before and after heating cycle.

A single crystal is held in the path of monochromatic radiations and is rotated about an axis, i.e., λ is fixed while θ varies. Different sets of parallel atomic planes are exposed to incident radiations for different values of θ and reflections take place from those atomic planes for which d and θ satisfy the Bragg's law. This method is known as the *rotating crystal method*.

3. The powder method

This technique employs monochromatic radiation and a finely powdered, or fine-grained polycrystalline specimen. In this case, a fixed beam's wavelength is used with a varying angle; this method can be used to determine lattice parameters accurately.

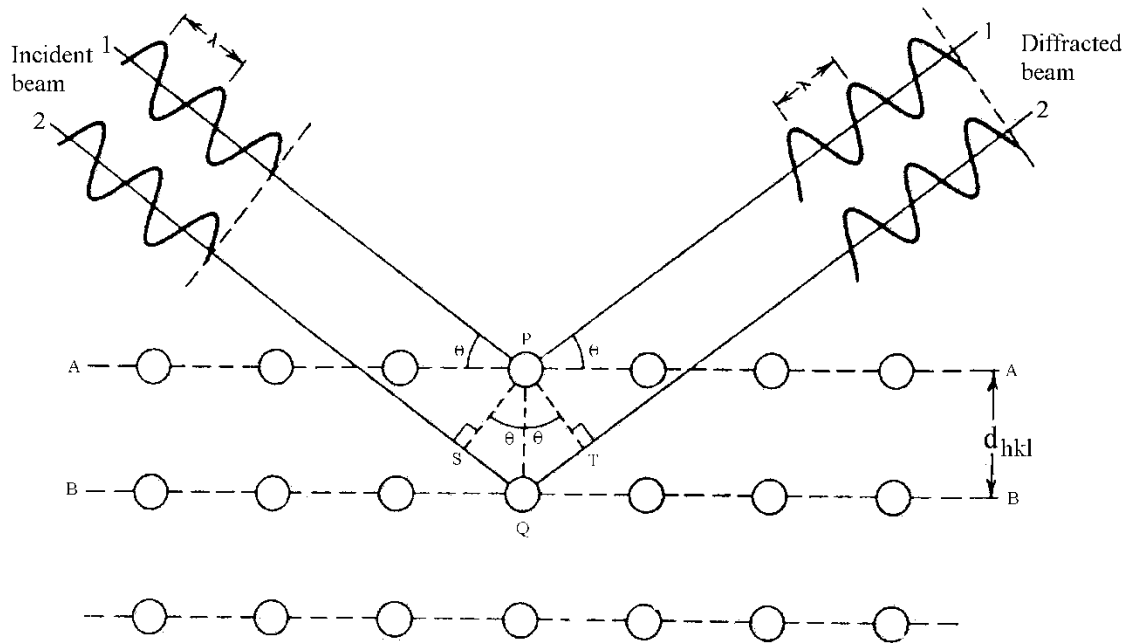


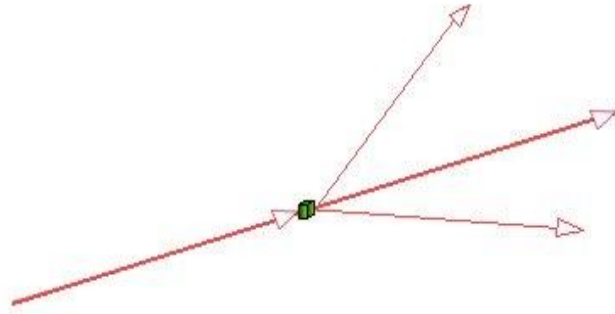
Fig. 4.1 Diffraction of X-ray by planes of atoms

4.3 X-Ray Powder Diffraction

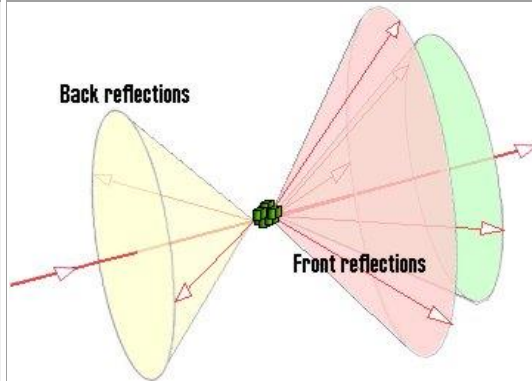
The sample in the powdered form is placed in the path of monochromatic x-rays , i.e., λ is fixed while both θ and d vary. Thus a number of small crystallites with different orientations are exposed to x-rays. The reflections take place for those values of d , θ and λ which satisfy the Bragg's law. This method is called the *powder method*.

The powder method is used to determine the value of the lattice parameters accurately. Lattice parameters are the magnitudes of the unit vectors **a**, **b** and **c** which define the unit cell for the crystal.

If a monochromatic x-ray beam is directed at a single crystal, then only one or two diffracted beams may result.

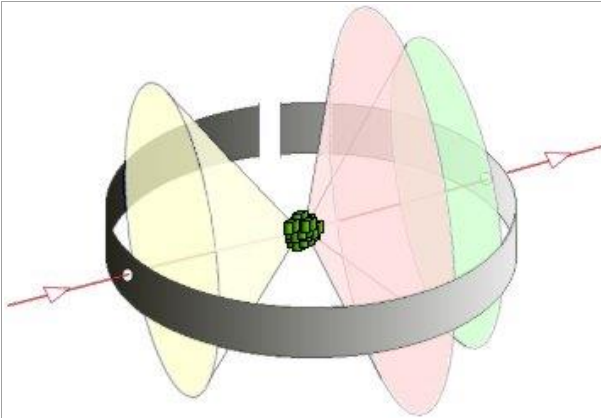


If the sample consists of some tens of randomly orientated single crystals, the diffracted beams are seen to lie on the surface of several cones. The cones may emerge in all directions, forwards and backwards.



A sample of some hundreds of crystals (i.e. a powdered sample) show that the diffracted beams form continuous cones.

A circle of film is used to record the diffraction pattern as shown. Each cone intersects the film giving diffraction lines. The lines are seen as arcs on the film.



The periodic structure of crystals at the atomic level effects their macroscopic properties; X-ray powder diffraction is an old technique, in use for most of this century. The capabilities of the technique have recently grown for two main reasons: (1) development of x-ray sources and optics and (2) the increasing power of computers and software for analysis of powder data. Their physical properties are orientation dependent. A simpler way to describe the geometry (but not intensity) of diffraction is using Bragg's law.

X-ray powder diffraction is used to determine the atomic structure of crystalline materials without the need for large (~100- mm) single crystals. “Powder” can be a misnomer; the technique is applicable to polycrystalline phases such as cast solids or films grown on a substrate. X-ray powder diffraction can be useful in a wide variety of situations. Below is a list of a number of questions that can be effectively addressed by this technique.

1. The positions and integrated intensities of a set of peaks in an x-ray powder diffraction pattern can be compared to a database of known materials in order to identify the contents of the sample and to determine the presence or absence of any particular phase.
2. A mixture of two or more crystalline phases can be easily and accurately analyzed in terms of its phase fractions, whether or not the crystal structures of all phases are known. This is called quantitative phase analysis, and it is particularly valuable if some or all of the phases are chemically identical and hence cannot be distinguished while in solution.
3. The crystal structure of a new or unknown material can be determined when a similar material with a known structure exists. Depending on the degree of similarity between the new and the old structure, this can be fairly straightforward.
4. The crystal structure of a new or unknown material can be solved *ab initio* even if no information about the material other than its stoichiometry is known. This case is significantly more difficult than the previous one, and it requires both high-resolution data and a significant investment of time and effort on the part of the investigator.
5. Phase transitions and solid-state reactions can be investigated in near real time by recording x-ray powder diffraction patterns as a function of time, pressure, and/or temperature.
6. Subtle structural details such as lattice vacancies of an otherwise known structure can be extracted. This also usually requires high-resolution data and a very high sample quality.

X-ray powder diffraction is an old technique, in use for most of this century. The capabilities of the technique have recently grown for two main reasons: (1) development

of x-ray sources and optics (e.g., synchrotron radiation, Göbel mirrors) and (2) the increasing power of computers and software for analysis of powder data. This unit discusses the fundamental principles of the technique, including the expression for the intensity of each diffraction peak, gives a brief overview of experimental techniques, describes several illustrative examples, gives a description of the procedures to interpret and analyze diffraction data, and discusses weaknesses and sources of possible errors.

4.4 Practical Aspects of the Method

Most laboratory powder x-ray diffractometers use a sealed x-ray tube with a target of copper, molybdenum, or some other metal. About half of the x-rays from such a tube are in the characteristic K_α line ($\lambda = 1.54 \text{ \AA}$ for Cu, $\lambda = 0.70 \text{ \AA}$ for Mo), and the remainder are in other lines and in a continuous bremsstrahlung spectrum.

There are a large number of detectors suitable for powder x-ray diffraction. Perhaps the simplest is photographic film, which allows the collection of an entire diffractogram at one time and, with proper procedures, can be used to obtain quantitative intensities with a dynamic range up to 100:1 (Klug and Alexander). The simplest electronic detector, the Geiger counter, is no longer widely used because of its rather long dead time, which limits the maximum count rate. The gas-filled proportional counter offers higher count rates and some degree of x-ray energy resolution. The most widely used x-ray detector today is the scintillation counter, in which x-rays are converted into visible light, typically in a thallium-doped NaI crystal, and then into electronic pulses by a photomultiplier tube. Various semiconductor detectors [Si:Li, positive-intrinsic-negative (PIN)] offer energy resolutions of 100 to 300 eV, sufficient to distinguish fluorescence from different elements and from the diffracted x-rays, although their count rate capability is generally lower than that of scintillation counters.

Some of the most important configurations for x-ray powder diffraction instruments are illustrated in Fig 4.2. The simple Debye-Scherrer camera in (A) records a wide range of angles on curved photographic film but suffers from limited resolution. Modern incarnations include instruments using curved position-sensitive detectors and imaging plates and are in use at several synchrotron sources. It generally requires a thin rod-shaped sample either poured as a powder into a capillary or mixed with an appropriate

binder and rolled into the desired shape. The Bragg-Brentano diffractometer illustrated in (B) utilizes parafocusing from a flat sample to increase the resolution available from a diverging x-ray beam; in this exaggerated sketch, the distribution of Bragg angles is 3° , despite the fact that the sample subtends an angle of 15° from source or detector. The addition of a diffracted-beam monochromator illustrated in (C) produces a marked improvement in performance by eliminating x-ray fluorescence from the sample. For high-pressure cells, with limited access for the x-ray beam, the energy-dispersive diffraction approach illustrated in (D) can be an attractive solution. A polychromatic beam is scattered through a fixed angle, and the energy spectrum of the diffracted x-rays is converted to d spacings for interpretation.

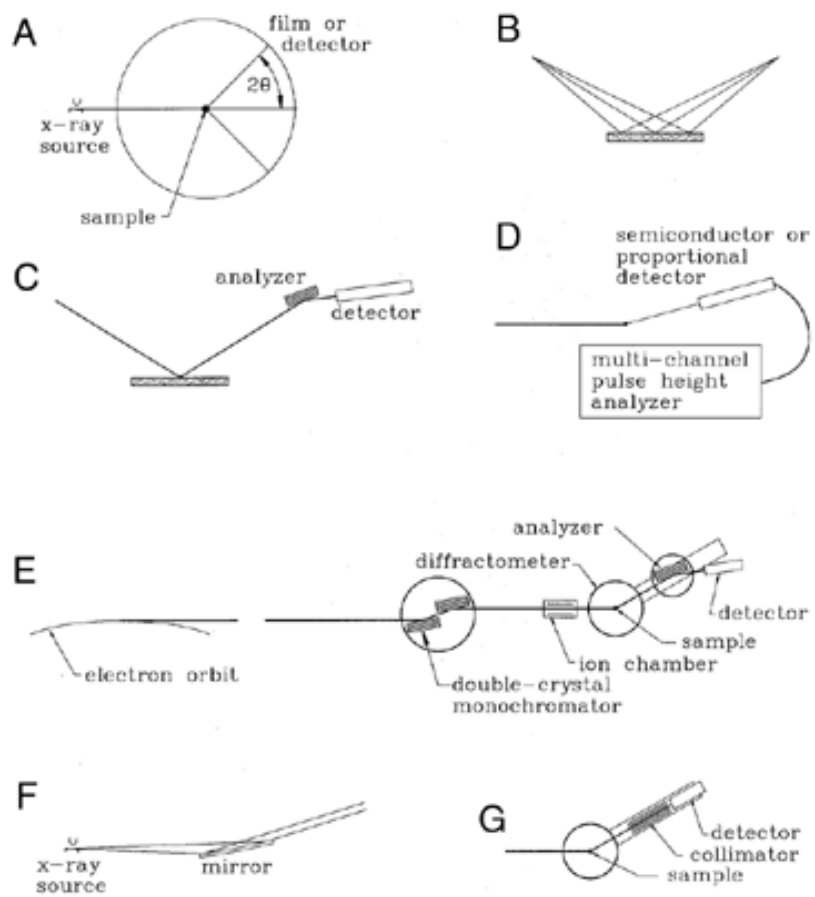


Fig 4.2 Schematic illustration of experimental setups for powder diffraction measurements.

A typical synchrotron powder beam line such as X7A or X3B1 at the National Synchrotron Light Source (Brookhaven National Laboratory) is illustrated in (E). One particular wavelength is selected by the dual-crystal monochromator, and the x-rays are diffracted again from an analyzer crystal mounted on the 2θ arm. Monochromator and analyzer are typically semiconductor crystals with rocking-curve widths of a few thousandths of a degree. Besides its intrinsically high resolution, this configuration offers the strong advantage that it truly measures the angle through which a parallel beam of radiation is scattered and so is relatively insensitive to parallax or sample transparency errors.

The advantage of a parallel incident beam is available on laboratory sources by the use of a curved multilayer (Göbel) mirror (F), currently commercialized by Bruker Analytical X-ray Systems. One can also measure the diffracted angle, free from parallax, by use of a parallel-blade collimator as shown in (G). This generally gives higher intensity than an analyzer crystal at the cost of coarser angular resolution (0.1° to 0.03°), but this is often not a disadvantage because diffraction peaks from real samples are almost always broader than the analyzer rocking curve. However, the analyzer crystal also discriminates against fluorescence.

There are a number of sources of background in a powder diffraction experiment. X-rays can be scattered from the sample by a number of mechanisms other than Bragg diffraction: Compton scattering, thermal diffuse scattering, scattering by defects in the crystal lattice, multiple scattering in the sample, and scattering by noncrystalline components of the sample, by the sample holder, or even by air in the x-ray beam path. The x-rays scattered by all of these mechanisms will have an energy that is identical to or generally indistinguishable from the primary beam, and so it is not possible to eliminate these effects by using energy-sensitive detectors. Another important source of background is x-ray fluorescence, the emission of x-rays by atoms in the target that have been ionized by the primary x-ray beam. X-ray fluorescence is always of a longer wavelength (lower energy) than the primary beam and so can be eliminated by the use of a diffracting crystal between sample and detector or an energy-sensitive detector (with

the precaution that the fluorescence radiation does not saturate it) or controlled by appropriate choice of the incident wavelength.

4.5 Data Analysis and Interpretation

A very important technique for analysis of powder diffraction data is the whole-pattern fitting method proposed by Rietveld. It is based on the following properties of x-ray (and neutron) powder diffraction data: a powder diffraction pattern usually comprises a large number of peaks, many of which overlap, often very seriously, making the separate direct measurement of their integrated intensities difficult or impossible. However, it is possible to describe the shape of all Bragg peaks in the pattern by a small (compared to the number of peaks) number of profile parameters. This allows the least-squares refinement of an atomic model combined with an appropriate peak shape function, i.e., a simulated powder pattern, directly against the measured powder pattern. This may be contrasted to the single-crystal case, where the atomic structure is refined against a list of extracted integrated intensities.

The parameters refined in the Rietveld method fall into two classes: those that describe the shape and position of the Bragg peaks in the pattern (profile parameters) and those that describe the underlying atomic model (atomic or structural parameters). The former include the lattice parameters and those describing the shape and width of the Bragg peaks. In x-ray powder diffraction, a widely used peak shape function is the pseudo-Voigt function (Thompson *et al.*), a fast-computing approximation to a convolution of a Gaussian and a Lorentzian (Voigt function). It uses only five parameters (usually called U, V, W, X , and Y) to describe the shape of all peaks in the powder pattern. In particular, the peak widths are a smooth function of the scattering angle 2θ . Additional profile parameters are often used to describe the peak asymmetry at low angles due to the intersection of the curved Debye-Scherrer cone of radiation with a straight receiving slit and corrections for preferred orientation. The structural parameters include the positions, types, and occupancies of the atoms in the structural model and isotropic or anisotropic thermal parameters (Debye-Waller factors). The power of the Rietveld method lies in simultaneous refinement of both profile and atomic parameters, thereby maximizing the amount of information obtained from the powder data.

4.6 Crystal Lattice and Space Group Determination from X-Ray

Powder Data

Obtaining the lattice parameters (unit cell) of an unknown material is always the first step on the path to a structure solution. While predicting the scattering angles of a set of diffraction peaks given the unit cell is trivial, the inverse task is not, because the powder method reduces the three-dimensional atomic distribution in real space to a one-dimensional diffraction pattern in momentum space. Once the unit cell is known, the space group can be determined from systematic absences of Bragg peaks, i.e., Bragg peaks allowed by the unit cell but not observed in the actual spectrum. For example, the observed spectrum of a face-centered-cubic (fcc) material contains only Bragg peaks (hkl) for which h , k , and l are either all odd or all even. Tables listing possible systematic absences for each crystal symmetry class and correlating them with space groups can be found in the International Tables for Crystallography (Vos and Buerger).

When a suitable starting model for a crystal structure is not known and cannot easily be guessed, it must be determined from the x-ray powder data before any Rietveld refinements can be performed. The Fourier transform of the distribution of electrons in a crystal is the x-ray scattering amplitude. However, only the scattering intensity can be measured, and hence all phase information is lost. Nevertheless, the Fourier transform of the intensities can be useful in finding some of the atoms in the unit cell. A plot of the Fourier transform of the measured scattering intensities is called a Patterson map, and its peaks correspond to translation vectors between pairs of atoms in the unit cell.

4.7. Sample Preparation

The preparation of samples to avoid unwanted artifacts is an important consideration in powder diffraction experiments. One issue is that preferred orientation (texture) should be avoided or controlled. The grains of a sample may tend to align, especially if they have a needle or plate like morphology, so that reflections in certain directions are enhanced relative to others. Various measures such as mixing the powder with a binder or an inert material chosen to randomize the grains or pouring the sample sideways into the flat plate sample holder are in common use. It is also possible to correct experimental data if one

can model the distribution of crystallite orientations; this option is available in most common Rietveld programs.

However, grinding can introduce strain broadening into the pattern, and some experimentation is usually necessary to find the optimum means of preparing a sample. A useful test of whether a specimen in a diffractometer is sufficiently powdered is to scan the sample angle θ over several degrees while leaving 2θ fixed at the value of a strong Bragg peak, in steps of perhaps 0.01° ; fluctuations of more than a few percent indicate trouble. It is good practice to rock (flat plate) or twirl (capillary) the sample during data collection to increase the number of observed grains.

In as much as a powder diffraction experiment consists of “simply” measuring the diffracted intensity as a function of angle, one can classify sources of systematic error as arising from measurement of the intensity or the angle or from the underlying assumptions. Errors of intensity can arise from detector saturation, drift or fluctuations of the strength of the x-ray source, and the statistical fluctuations intrinsic to counting the random arrival of photons.

Error of the angle can arise from mechanical faults or instability of the instrument or from displacement of the sample from the axis of the diffractometer (parallax). A subtle form of parallax can occur for flat-plate samples that are moderately transparent to x-rays, because the origin of the diffracted radiation is located below the surface of the sample by a distance that depends on the diffraction angle. Another effect that can give rise to an apparent shift of diffraction peaks is the asymmetry caused by the intersection of the curved Debye-Scherrer cone of radiation with a straight receiving slit. This geometric effect has been discussed by several authors and it can produce a significant shift in the apparent position of low-angle peaks if fitted with a model lineshape that does not properly account for it. So that the observed Bragg angle is slightly shifted from its value inside the sample.

There are a number of standard samples that are useful for verifying and monitoring instrument performance and as internal standards. Silver behenate powder has been proposed as a useful standard with a very large lattice spacing of $c = 58.4 \text{ \AA}$.

4.8 Comparison Against a Database of Known Materials

An ongoing investigation of novel carbon materials yielded a series of samples with new and potentially interesting properties: (1) the strongest signal in a mass spectrometer was shown to correspond to the equivalent of an integer number of carbon atoms, (2) electron diffraction indicated that the samples were at least partially crystalline, and (3) while the material was predicted to consist entirely of carbon, the procedures for synthesis and purification had involved an organic Li compound. The Powder Diffraction File (PDF) database provided by the International Center for Diffraction Data (ICDD, 1998) allows for searching based on several search criteria, including types of atoms, positions of Bragg peaks, or unit cell parameters. Note that it is not necessary to know the unit cell of a compound to search the database against its diffraction pattern, nor is it necessary to know the crystal structures (or even the unit cells) of all the compounds included in the database.

Searches for materials with an appropriate position of their strong diffraction peaks containing C only, or containing some or all of C, N, O, or H, did not result in any candidate materials. The peak intensities listed in the database, converted to 2θ for the appropriate wavelength. This type of experiment is fairly simple, and both data collection and analysis can be performed quickly. Average sample quality is sufficient, and usually so are relatively low-resolution data from an x-ray tube. In fact, this test is routinely performed before any attempt to solve the structure of an unknown and presumably new material.

4.9 Quantitative Phase Analysis

Quantitative phase analysis refers to the important technique of determining the amount of various crystalline phases in a mixture. It can be performed in two ways, based on the intensities of selected peaks or on a multiphase Rietveld refinement. In the first case, suppose that the sample is a flat plate that is optically thick to x-rays. In a mixture of two phases with mass absorption coefficients μ_1^* and μ_2^* (cm^2/g), the intensity of a given peak from phase 1 will be reduced from its value for a pure sample of phase 1 by the ratio

$$\frac{I_1(x_1)}{I_1(\text{pure})} = \frac{x_1\mu_1^*}{x_1\mu_1^* + (1-x_1)\mu_2^*} \quad (4.6)$$

where x_1 is the weight fraction of phase 1. Note that the intensity is affected both by dilution and by the change of the sample's absorption constant. When the absorption coefficients are not known, they can be determined from experimental measurements, such as by “spiking” the mixture with an additional amount of one of its constituents. Details are given in Klug and Alexander and Bish and Post.

If the atomic structures of the constituents are known, a multiphase Rietveld refinement (see above) directly yields scale factors s_j for each phase. The weight fraction w_j of the j th phase can then be calculated by

$$\omega_j = \frac{s_j Z_j m_j V_j}{\sum_i s_i Z_i m_i V_i} \quad (4.7)$$

where Z_j is the number of formula units per unit cell, m_j is the mass of a formula unit, and V_j is the unit cell volume.

In either case, the expressions above are given under the assumption that the powders are sufficiently fine, i.e., the product of the linear absorption coefficient m (cm^{-1} , equal to m^* r) and the linear particle (not sample) size D is small ($mD < 0.01$). If not, one must make allowance for microabsorption, as described by Brindley.

It is worth noting that the sensitivity of an x-ray powder diffraction experiment to weak peaks originating from trace phases is governed by the signal-to-background ratio. Hence, in order to obtain maximum sensitivity, it is desirable to reduce the relative background as much as possible.

The qualitative and quantitative detection of small traces of polymorphs plays a major role in pharmacology, since many relevant molecules form two or more different crystal structures, and phase purity rather than chemical purity is required for scientific, regulatory, and patent-related legal reasons. Mixtures of the α and γ phases of the anti-inflammatory drug indomethacin ($\text{C}_{19}\text{H}_{16}\text{ClNO}_4$) provide a good example for the

detection limit of x-ray powder diffraction experiments in this case (Dinnebier *et al.*) Mixtures of 10, 1, 0.1, 0.01, and 0 wt% α phase (with the balance γ phase) were investigated. Using its five strongest Bragg peaks, 0.1% α phase can easily be detected, and the fact that the “pure” γ phase from which the mixtures were prepared contains traces of α became evident, making the quantification of the detection limits below 0.1% difficult.

4.10 Introduction to Crystallography

Crystallography is the branch of the exact sciences that studies the structure of matter on an atomic scale; the determination, classification and interpretation of the geometrical structure of solid and, in particular, those of crystal.

Crystallography plays an interdisciplinary role between Physics, Chemistry, Molecular biology, and Mineralogy – petrography .The geometrical foundations of Solid State Physics the determination of the microscopic structure to atomic resolution of inorganic, organic and macromolecular substances, the identification of substances and mixtures of substances, texture analysis in rocks and alloys as well as the alignment and orientation control of crystals are all endeavors that call upon crystallography . The principal experimental method used is the diffraction by crystals of X rays or neutrons. Since 1960, X rays crystallography has blossomed with the development of more and more powerful compute. Today, more than 9000 crystal structures are published each year, along with 2000 new power diagrams. Nineteenth – century crystallography may be considered to be the mathematical branch of mineralogy.

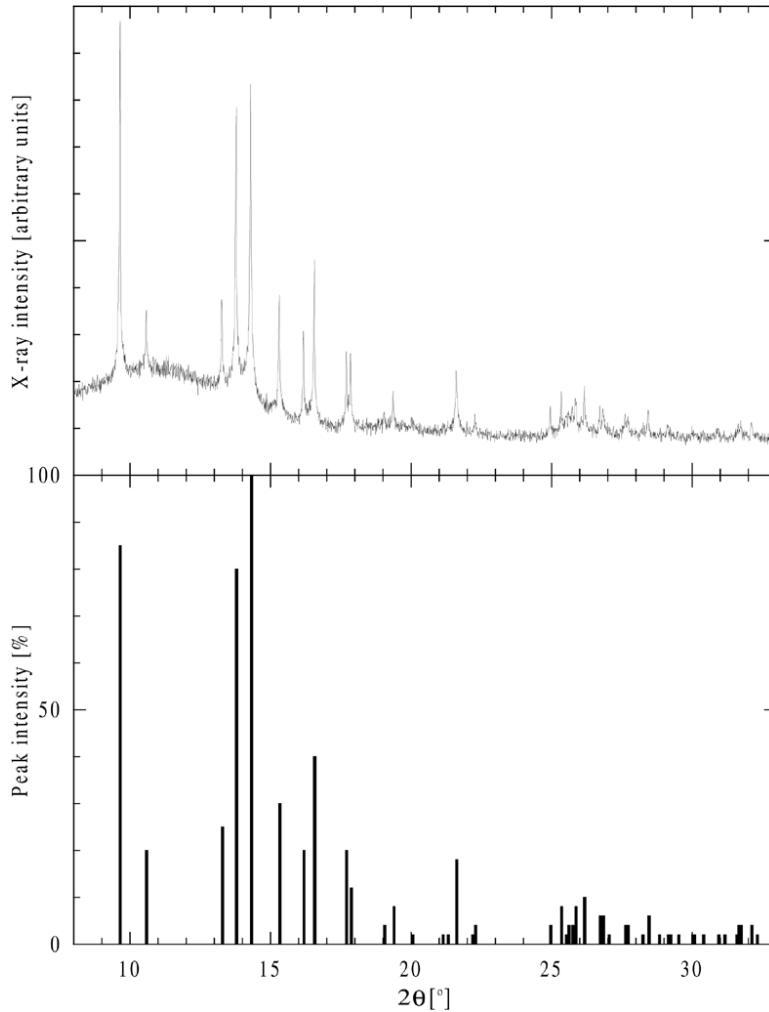


Fig 4.3 X-ray powder diffraction pattern of “unknown” sample (top) and relative peak intensities of Li_2O_3 as listed in the PDF database (bottom), both at $\lambda = 0.7 \text{ \AA}$.

4.11 Crystal Systems

A crystal is a solid whose microscopic structure is characterized by a periodic repetition in three dimensions of a motif composed of atoms. Crystals have ordered structures and the study of order and disorder is a central preoccupation of the crystallographer.

Space was divided by three sets of planes. If the planes in the three sets are equally spaced and mutually perpendicular, the unit cell is cubic. In this case the vectors a , b , c are all equal and at right angles to one another, or $a=b=c$ and $\alpha=\beta=\gamma=90^\circ$. By thus giving special values to the axial lengths and angles, we can produce unit cells of various shapes

and therefore various kinds of point lattices, since the points of the lattice are located at the cell corners. It turns out that only seven different kinds of cells are necessary to include all the possible point lattices. These correspond to the seven crystal systems into which all crystals can be classified. These systems are listed in Table 4.1. Seven different point lattices can be simply by putting points at the corners of the unit cells of the seven crystal systems. However, there are other arrangements of points which fulfill the requirements of a point lattice, namely, that each point have identical surroundings.

If a point is placed at the center of each cell of a cubic point lattice, the new array of points also forms a point lattice. Similarly, another point lattice can be based on a cubic unit cell having lattice points at each corner and in the center of each face. The fourteen Bravais lattices are described in Table 4.1 and illustrated in Fig 4. 4, where the symbols P,F,I etc., have the following meanings. We must first distinguish between simple, or primitive, cells and nonprimitive cells. Primitive cells have only one lattice point per cell while nonprimitive have more than one. A lattice point in the interior of a cell "belongs" to that cell, while one in a cell face is shared by two cells and one at a corner is shared by eight. The number of lattice points per cell is therefore given by

$$N = N_i + N_f / 2 + N_c / 8 \quad (4.8)$$

where N_i = the number of interior points, N_f = the number of points on faces, and N_c = the number of points on corners. Any cell containing lattice points on the corners only is therefore primitive, while one containing additional points in the interior or on faces is nonprimitive. The symbols F and I refer to face –centered and body-centered cells, respectively, while A,B and C refer to base-centered cells, centered on one pair of opposite faces A,B or C. The symbol R is used especially for the rhombohedral system. In Fig 4.4, the axes of equal length in a particular system are given the same symbol to indicate their equality.

4.12 Diffraction of X rays by Crystal

X-rays are electromagnetic waves just like visible light. They interact with the electrons contained in all matter. In crystallography, we use X-rays with wavelength of the order of 0.5 to 2Å. In a solid, the interatomic distances are of the order of an angstrom ($1\text{Å} = 10^{-10}$

m = 100 pm). In first step we measured the radiation diffracted by the sample. Due to their symmetry properties and in particular to the periodicity of their structures, the diffraction pattern produced by crystals is especially simple.

4.12.1 Experimental Set-up

In instruments, essentially monochromatic radiation is used and the x ray detector is placed on the circumference of a circle centered on the powder specimen. The essential features of a diffractometer are shown in Fig 4.5. A powder specimen C, in the form of a flat plate, is supported on a table H, which can be rotated about an axis O perpendicular to the plane of the drawing. The x ray source is S, the line focal spot on the Cu target T of the x ray tube; S is also normal to the plane of the drawing and therefore parallel to the diffractometer axis O. X rays diverge from this source and are diffracted by the specimen to form a convergent diffracted beam which comes to a focus at the slit F and then enters the counter G. A and B are special slits which define and collimate the incident and diffracted beams.

A high resolution x ray powder diffraction pattern of a sample of $C_5H_8NNaO_4H_2O$ was measured at room temperature, wavelength of Cu K- α radiation $\lambda = 1.54056 \text{ \AA}$ (Cu/K-alpha) and $2\theta = 5^\circ$ to 80° with step size 4° . A total counting time (or) exposure time 18.75 minute. The x-ray diffractometer used throughout this investigation is a computer-controlled Rigaku, the model number is D/max-2200/-PC and Cat number G 402. The operation conditions of the x-rays diffractometer using copper target. The operation tube voltage 40kV and 30mA tube current. The detection unit is NaI scintillation detector. The block diagram of the experimental set up was shown in Fig 4.6.

Table 4.1 Crystal Systems and bravais lattices

System	Axials lengths and angles	Bravais lattice	Lattice symbol
Cubic	Three equal axes at right angles $A=b=c, \alpha=\beta=\gamma=90^\circ$	Simple	P
		Body-centered	I
		Face-centered	F
Tetragonal	Three axes at right angles, two equal $a=b\neq c, \alpha=\beta=\gamma=90^\circ$	Simple	P
		Body-centered	I
Orthorhombic	Three unequal axes at right angles $a\neq b\neq c, \alpha=\beta=\gamma=90^\circ$	Simple	P
		Body-centered	I
		Base-centered	C
		Face-centered	F
Rhombohedral	Three equal axes, equally inclined $a=b=c, \alpha=\beta=\gamma\neq 90^\circ$	Simple	R
Hexagonal	Two equal coplanar axes at 120° , third axis at right angles $a=b\neq c, \alpha=\beta=90^\circ, \gamma=120^\circ$	Simple	P
Monoclinic	Three unequal axes, one pair not at right angles $a\neq b\neq c, \alpha=\gamma=90^\circ\neq\beta$	Simple	P
		Base-centered	C
Triclinic	Three unequal axes, unequally inclined and none at right angles $a\neq b\neq c, \alpha\neq\beta\neq\gamma\neq 90^\circ$	Simple	P

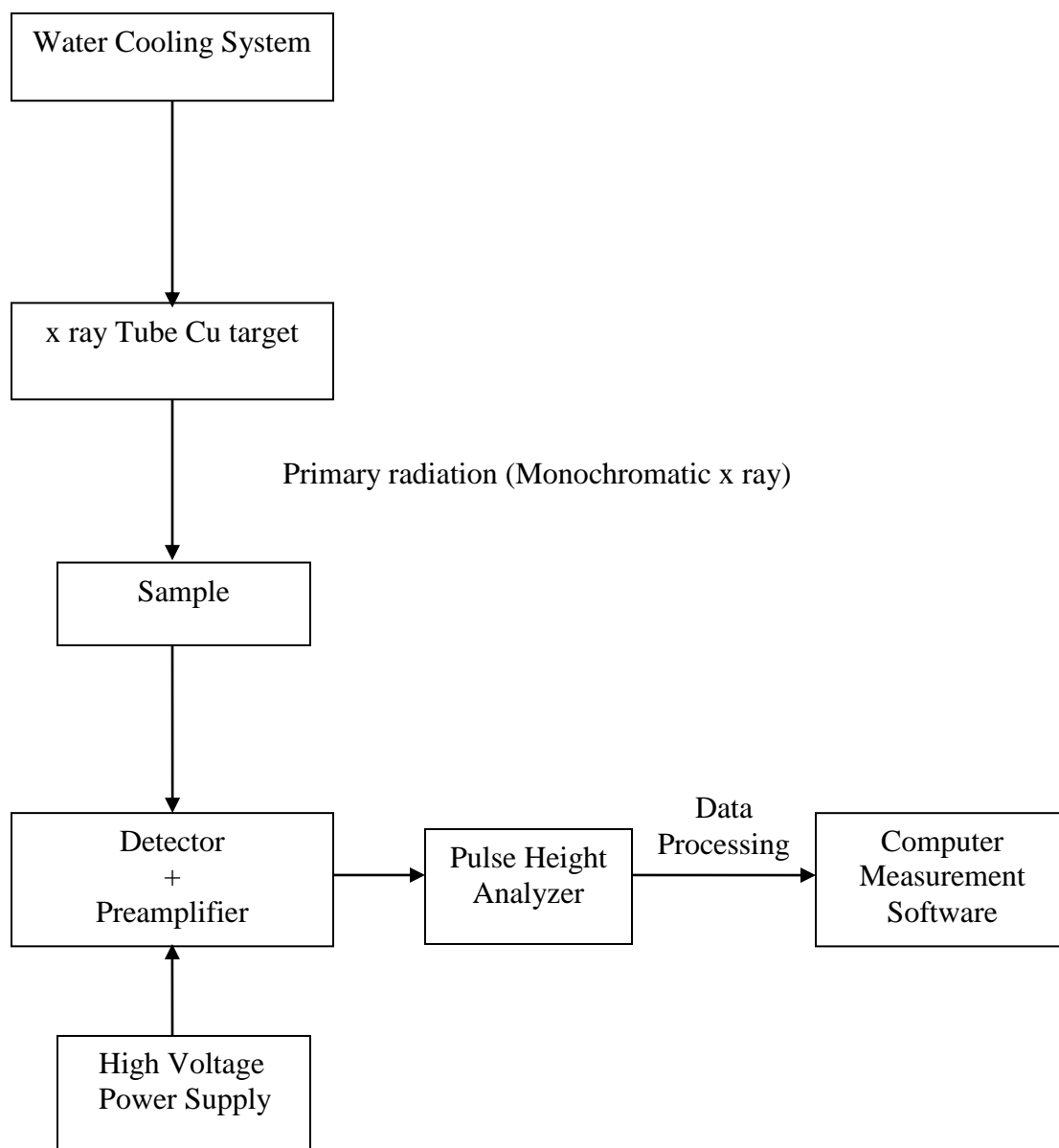


Fig 4.6 Block diagram of x rays diffractometer system

4.13 Results and Discussion

Qualitative analysis on powdered samples of MSG is performed by using Regaru powder diffractometer. X rays radiated from the X ray tube with a copper target is rest rained by divergence slit(DS) and hit the powdered sample placed in the center of goniometer. The X ray diffracted beam from the specimen is focused on the receiving slit(RS) placed in the position opposite to the X ray focus in relation to the sample.

The diffracted X ray is received by a X ray detector such as scintillation counter and converted to electric signals, and then recorded on a strip chart recorder by the counting rate (counts per second) can be measured recording, the measured sample .

All the peak heights and peak position are good agreement with **JCPDS**(Joint Committee on Powder Diffraction Standards)file data for MSG. In the JCPDS X ray power data fills the diffractio pattern of the material is identical by the interplanar spacing d , corresponding to each diffraction line and the relative intensity of the diffracted X ray .The X ray diffractometer recording and X ray power data file of diffracted beams from MSG material are shown in Fig 4.7 and table 4.2 respectively. The Powder method is also used for identifying substance. The (JCPDS)data bank contains all the difftrograms published in the scientific literature and provides the computer software and the bibliographic data to compare them with that of a unknown substance.

CHAPTER V

STRUCTURAL AND VIBRATIONAL ANALYSIS

5.1 Sample preparation

MSG single crystal was recrystallized by slow evaporation of aqueous solution containing 20g of MSG and 25cc of H₂O. The solution is filtered into a beaker is then covered and set aside for a few days. Crystals are placed on filter paper to dry. The transparent MSG crystals, were selected for FTIR, Raman Scattering and XRD measurements.

5.2 FTIR Spectroscopy

The IR transmission spectrum of the MSG crystal was recorded in the middle wave number ranges: 400 -4000 cm⁻¹ by means of Fourier Transform Infrared Spectrometer (FTIR - 8400 Shimadzu). The resolution was 4 cm⁻¹ and the number of scans was fixed to 45. Single beam spectra contain also additional features due to the instrument and the environment.

As shown in Fig 5.1, the FTIR - 8400 relies on a Michelson Interferometer with the Ceramic Light Source, which is electrically heated. After passing through the aperture, light is turned into a parallel by the collimator mirror and enters the beam splitter. A germanium film, deposited on a potassium bromide substrate via evaporation, comprises the beam splitter; it splits the single beam into two, reflecting one to the fixed mirror and transmitting the other to the moving mirror. Both mirrors reflect their beams back to the beam splitter; part of each returning beam is reflected and transmitted. The transmitted light from the fixed mirror and the reflected light from the mirror recombine and interfere with each other as they travel towards the converging mirror. Interference is either constructive or destructive.

From the converging mirror, the parallel infrared beam creates an image of the light source in the center of the sample compartment. Collecting mirror gathers the beam that passed through the sample and reflects it to a pyroelectric detector DLATGS as the interferogram. After reaching the detector, the interferogram undergoes several treatments before being sent to the computer. It is amplified by the preamplifier and the automatic gain amplifier, passes through high-pass and low-pass filters, and is digitized

by the 20-bit A/D converter. After the signal is digitized into the interferometer memory, it travels through the SCSI interface to the PC where Hyper-IR Software transforms the interferogram into a spectrum.

The Fourier Transform (FT) process is most easily visualized in terms of the emission of radiation. The technique can also be applied to absorption. A ‘white’ source would show a single decay signal with no beats; an approximation to this is shown in Fig 5.2 (a), where a very broad emission line (which can be considered as a white source covering a limited region of the spectrum) and its Fourier transform are shown. Although the time domain signal decays very rapidly, it does show some beats; this is because the broad emission line is only an approximation to a proper white source. We can now imagine an absorbing sample making some ‘holes’ in this radiation, as shown on the left-hand side of Fig 5.2 (b), with its resulting FT signal on the right. Although we may find it difficult to imagine Fourier - transforming (or even just adding up) the absence of radiation at some frequencies, in practice a detector will collect a perfectly sensible signal which can be stored by a computer, transformed, and displayed as the normal absorption spectrum.

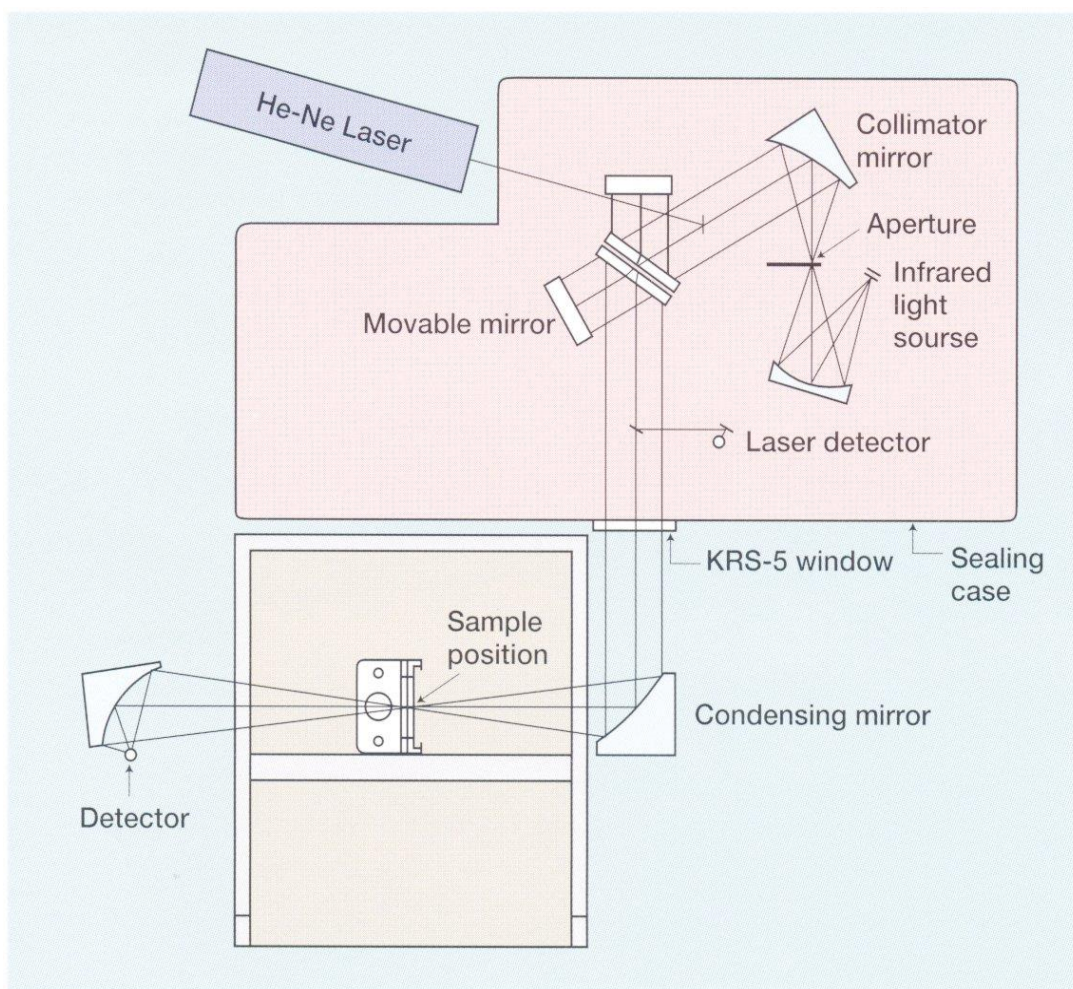


Fig 5.1 Schematic diagram of the FTIR system

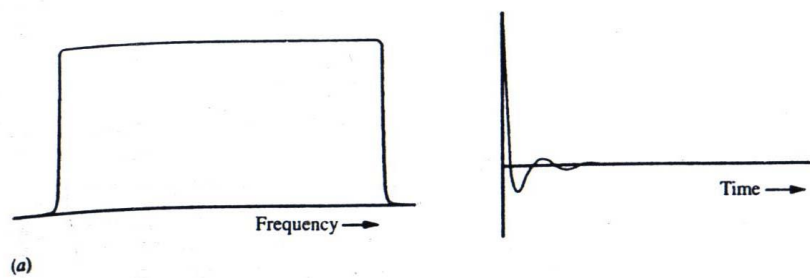


Fig 5.2 (a) An approximation to a 'white' source and its Fourier transform

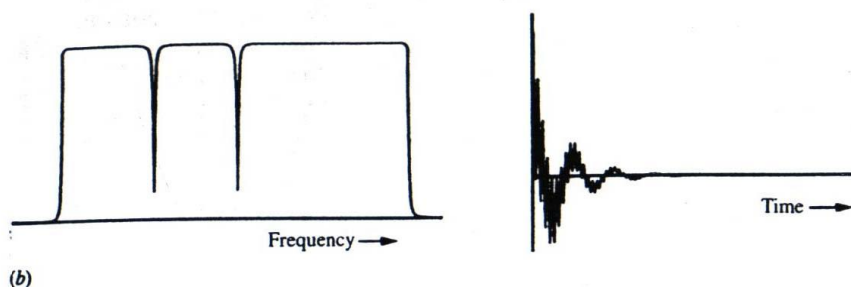


Fig 5.2 (b) Some absorptions from a 'white' source and their Fourier transform

5.3 Raman Spectroscopic System

Raman effect occurs because of a change in magnitude or direction of the electronic polarizability during the molecular motion, while infrared absorption occurs because of a change in magnitude or direction of the electric dipole moment during the motion. The magnitude of the induced dipole moment \mathbf{P} is given by $|\mathbf{P}| = \alpha |\mathbf{E}|$ where \mathbf{E} is the electric vector of the incident radiation frequency ν and α the polarizability. If α changes during the vibration i with frequency ν_i , \mathbf{P} will change with the frequencies $\nu + \nu_i$ and $\nu - \nu_i$ as well as with frequency ν . The scattered light will thus contain the frequencies $\nu \pm \nu_i$ in addition to ν . Therefore, the Raman record is obtained by spectral analysis of the light scattered from the sample illuminated by a laser source is shown in Fig 5.3; it has the form of the intensity I of the scattered light versus the displacement of the frequency from the incident laser frequency.

The laser beam emerging from the R-2001 laser output port or from the fiber optic probe is a solid-state diode laser (red laser). The laser is operated in continuous wave (cw) mode at 532 nm with a 100 mW-output power. In order to avoid the local heating of sample, and incident power at the sample was usually adjusted to be 30-40 mW. The orientation of the probe is perpendicular to the top surface of a sample. The focal length (5mm) of the probe is used as a distance away from the surface of the sample to the probe. This orientation minimizes reflections of the laser light from the sidewalls and bottom back into the probe's collection fiber.

The InPhotonics Raman probe utilizes micro-optic components for delivering for laser excitation source to the sample and for collection of scattered light resulting in a compact probe head that is fiber optically coupled to the laser source and spectrograph. The spot size of the laser varies with the transmission properties of the sample under measurement. Using a collection fiber that is twice the size of the excitation fiber ensures maximum signal collection of transparent as well as opaque materials.

Through the efficient use of bandpass, dichroic and edge filters for separating the excitation and scattered light, the probe utilizes a back scattering ($\theta = 180^\circ$) sampling geometry. The Raman probe backscattering collection geometry allows easy sample

alignment and provides optimum throughput because of the totally overlap between the excitation and collections cones.

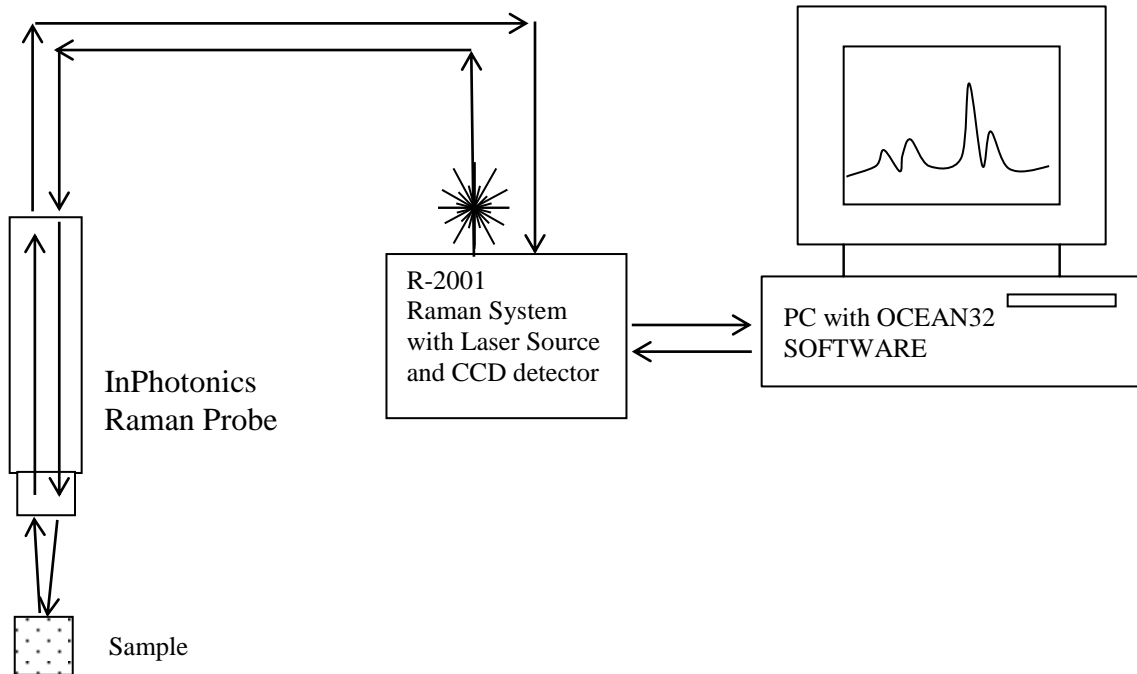


Fig 5.3 Raman Scattering Experimental set-up.

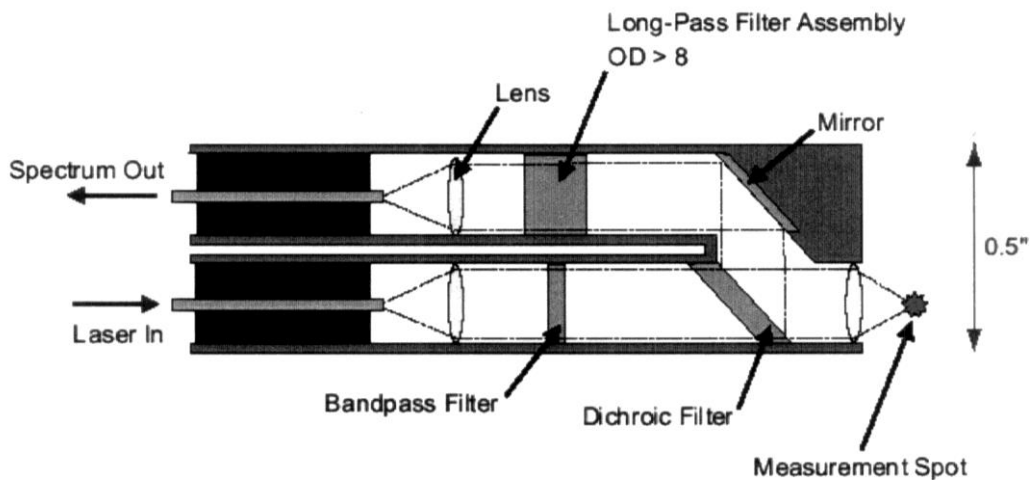


Fig 5.4 Internal optics of the InPhotonics Raman Probe.

The schematic diagram of the internal optics of the Raman probe is shown in Fig 5.4 The Raman Probe is coupled to the excitation source and the spectrograph via two optical fibers to allow remote measurements of samples. Each Fiber optic subunit is provided in a projective jacket. A specially designed fiber optic cable was built for the Raman probe that provides both protection to the optical fibers and also integrates electrical wires necessary to power up the probe LED safety. The fiber optic subunits and two 20 gauge hookup wires for the LED indicator are then woven together and encased in an external protective jacket. The jacketing material is a stainless-steel interlocking cable. The resulting cable has a diameter of nearly 0.25 inches and remains fairly flexible.

Each Raman vibrational band is characterized by its frequency, intensity, linewidth, and depolarization ratio. When the sample is a single crystal, it is possible to choose the orientations of the sample axes with respect to the incident beam so as to measure individual elements of the polarizability tensor. Group theory relates the point symmetry of the system at hand to these elements enabling one to characterize the molecular vibrations.

5.4 RESULT AND DISCUSSION

The IR spectrum was recorded in the middle wave number range of 400-4000 cm^{-1} by means of FTIR spectrometer (FTIR-8400 Shimadzu). The resolution was 4 cm^{-1} and the number of scans was fixed to 60. The IR spectrum and Raman spectrum of MSG crystal at room temperature is shown in Fig 5.5 and Fig 5.6. Raman spectroscopy is an appropriate tool for characterizing such proton transfer reactions.

Amino acids like methionine $\text{CH}_3\text{SCH}_2\text{CH}_2\text{CH}(\text{NH}_2)\text{CO}_2\text{H}$ actually do not exist in this natural form. Its Raman spectrum reveals no C=O stretching or $\nu(\text{NH}_2)$ stretching vibrations. On the contrary, for MSG, the observation of $\nu(\text{C}=\text{O})$ at 1631 cm^{-1} and $\nu(\text{NH}_2)$ at 3467 cm^{-1} attests to the presence of C=O and NH_2 in this compound.

Another vibration, mainly connected with C-C stretching vibration, around 940 cm^{-1} . In MSG, this vibration, appearing at 945 cm^{-1} . In the region of 3500-3300 cm^{-1} , the infrared spectrum is dominated by a very broad band arising from the stretching vibration of the N-H band of amine, where as the Raman spectrum shows two, strong lines associated with the vibrations of the CH and CH_2 groups. Both the infrared and Raman spectra have

two strong bands at 1404cm^{-1} and 1347cm^{-1} . These two band stretching vibrations of CH_2 groups.

Important bands and the conclusions are as under:

	Approximate frequency (cm^{-1})	Nature of Vibration
1	3467	N-H band of amine
2	1631	Conjugated COOH
3	1449	CH_2 scissoring
4	1404	CH_2 scissoring
5	1347	CH_2 wagging band progression
6	1289	CH_2 wagging band progression
7	1142	$\begin{array}{c} \\ -\text{C}-\text{N} \text{ (NH in amine)} \\ \end{array}$
8	1078	$\begin{array}{c} \\ -\text{C}-\text{O} \\ \end{array}$, $\nu(\text{C}=\text{S})$, S(in mono-)
9	999	$-\text{CH}=\text{CH}_2$, $\nu(\text{CC})$
10	933	C-C stretching vibration
11	627	$-\text{CH}=\text{CH}_2$; 40% $\text{O}=\text{C}=\text{N}$ bending

Mass no of COOH=45

Mass no of COONa=67

$$\nu \propto \frac{1}{\sqrt{m}}$$

ν = vibration frequency

m = mass no

$$\nu_{\text{COONa}} \propto \frac{1}{\sqrt{67}}$$

$$\nu_{\text{COOH}} \propto \frac{1}{\sqrt{45}}$$

$$\frac{\nu_{\text{COONa}}}{\nu_{\text{COOH}}} = \frac{\sqrt{45}}{\sqrt{67}} = 0.8195$$

$$\nu_{\text{COONa}} = 0.8195 \times 1631$$

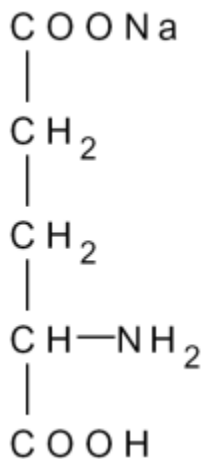
$$= 1334 \text{ cm}^{-1}$$

The observation of ν_{COOH} at 1631 cm^{-1} and ν_{COONa} at 1334 cm^{-1} confirm the presence of COOH and COONa in this compound.

Using the above information the compound may be assigned the structural formula as



(or)

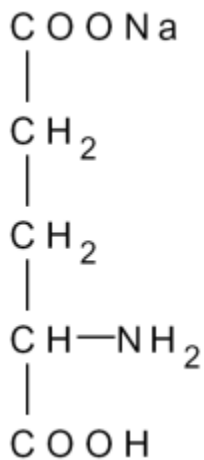


5.5 Conclusion

In this research, Na content 12.385% contain in MSG determined by NAA method. In EDXRF method, it was found that the major element is sodium only. But, the elements of sulphur (S), strontium (Sr), mercury (Hg), lead (Pb), arsenic (As) and scandium (Sc), which are known as toxic elements, were not found in this sample. Therefore, the above sodium glutamate is assumed to be safe in use. The Powder method is also used for identifying substance. All the peak heights and peak position are good agreement with JCPDS (Joint Committee on Powder Diffraction Standards) file data for MSG. In FTIR and Raman Spectroscopy, structural and nature of vibration can obtain approximate frequency. Therefore, light element in organic compound can be determine by FTIR and Raman Spectroscopy. Using the above information the compound may be assigned the structural formula as



(or)



REFERENCES

- [1] <http://www.fda.gov/opacom/backgrounders/msg.html>
- [2] <http://www.canberra.com/>
- [3] <http://www.lbl.gov/abc/wallchart/chapters/03/3.html/>
- [4] http://www.colorado.edu/physics/2000/x-rays/making_x-rays.html
- [5] Lipson H & Cochran W, 1966, The Determination of Crystal Structures (London: G Bell)
- [6] Hla Hla Than, PhD Thesis, 2002, Physics Department, Yangon University
- [7] Jenkins R, Gould R W & Gedcke D, 1981 Quantitative X-ray Spectrometry (New York: Marcell Dekker)
- [8] Gricken R E V, Marcowicz A A, 1981, Handbook of X-ray Spectrometry (New York: Marcell Deckker)
- [9] Instrumentation manual for NA pump type neutron generator 150-04 (Sussex: Multivolt)
- [10] Klug H P & Alexander L E, 1954, X-ray Diffraction Procedures (London: John Wiley)
- [11] Phillips J C, 1963, An Introduction To Crystallography (London: Longmans)
- [12] Buerger M J, 1965, X-ray Crystallography (London: John Wiley & Sons)
- [13] Enge H, 1966, Introduction to nuclear physics (London: Addison-Wesley)
- [14] Woolfson M M, 1970, An Introduction to X-Ray Crystallography (London: C U P)
- [15] Nargowalla S S & Przybylowicz E P, 1973, Activation Analysis with Neutron Generator (New York: John Wiley & Sons)
- [16] Kaplan I, 1971, Nuclear Physics (London: Addison-Wesley)
- [17] Knoll G F, 1979, Radiation Detection and Measurement (New York: John Wiley & Sons)
- [18] Edward A, 1979, Radiation Shielding and Dosimetry (New York: John Wiley & Sons)
- [19] Hamermesh M, 1989, Group Theory And Its Applications to Physics Problems (New York: Dover)
- [20] Helms H A, 1990, Semiconductor Radiation Detectors (Washington: Ann Arbor Science)